OXFORD GENETICS

GENETICS, 2023, 225(2), iyad149
https://doi.org/10.1093/genetics/iyad149
Advance Access Publication Date: 14 August 2023
Investigation

Caenorhabditis elegans NSE3 homolog (MAGE-1) is involved in genome stability and acts in inter-sister recombination during meiosis

Arome Solomon Odiba,[1,2,†] Guiyan Liao,[1,†] Chiemekam Samuel Ezechukwu,[1,6,†] Lanlan Zhang,[1,3] Ye Hong,[4] Wenxia Fang,[1] Cheng Jin,[1,2] Anton Gartner,[5] Bin Wang[1,*]

[1]State Key Laboratory of Non-food Biomass and Enzyme Technology, Guangxi Academy of Sciences, Nanning 530007, China
[2]State Key Laboratory of Mycology, Institute of Microbiology, Chinese Academy of Sciences, Beijing 100101, China
[3]College of Life Sciences, Hebei University, Baoding 071002, China
[4]Shandong Provincial Key Laboratory of Animal Cell and Developmental Biology, School of Life Sciences, Shandong University, Qingdao 266237, China
[5]IBS Center for Genomic Integrity, Department for Biological Sciences, Ulsan National Institute of Science and Technology, Ulsan 689-798, Republic of Korea
[6]Present address: Department of Zoology and Environmental Biology, University of Nigeria, Nsukka 410001, Nigeria

*Corresponding author: State Key Laboratory of Non-food Biomass and Enzyme Technology, Guangxi Academy of Sciences, Nanning 530007, China. Email: bwang@gxas.cn
[†]These authors contributed equally to this work.

Melanoma antigen (MAGE) genes encode for a family of proteins that share a common MAGE homology domain. These genes are conserved in eukaryotes and have been linked to a variety of cellular and developmental processes including ubiquitination and oncogenesis in cancer. Current knowledge on the MAGE family of proteins mainly comes from the analysis of yeast and human cell lines, and their functions have not been reported at an organismal level in animals. *Caenorhabditis elegans* only encodes 1 known MAGE gene member, *mage-1* (*NSE3* in yeast), forming part of the SMC-5/6 complex. Here, we characterize the role of *mage-1/nse-3* in mitosis and meiosis in *C. elegans*. *mage-1/nse-3* has a role in inter-sister recombination repair during meiotic recombination and for preserving chromosomal integrity upon treatment with a variety of DNA-damaging agents. MAGE-1 directly interacts with NSE-1 and NSE-4. In contrast to *smc-5*, *smc-6*, and *nse-4* mutants which cause the loss of NSE-1 nuclear localization and strong cytoplasmic accumulation, *mage-1/nse-3* mutants have a reduced level of NSE-1::GFP, remnant NSE-1::GFP being partially nuclear but largely cytoplasmic. Our data suggest that MAGE-1 is essential for NSE-1 stability and the proper functioning of the SMC-5/6 complex.

Keywords: *C. elegans*; DNA repair; meiosis; mitosis; *mage-1*; SMC-5/6 complex

Introduction

SMC (Structural Maintenance of Chromosomes) complexes are highly regulated ring-shaped protein complexes that encircle DNA and contribute to genomic integrity (Uhlmann 2016). In eukaryotes, 6 SMC proteins (Smc1–6) exist, and they interact in distinct combinations to form the cohesin (Smc1/3), condensin (Smc2/4), and the Smc5/6 complex (Uhlmann 2016). Cohesin mediates cohesion between newly replicated sister chromatids, while condensin condenses and compacts the chromosomes (Hagstrom and Meyer 2003; Skibbens 2019; Golfier *et al.* 2020). The Smc5/6 complex is implicated in a number of important cellular functions related to genome integrity during mitosis and meiosis (Toraason *et al.* 2022), which has been analyzed in a variety of organisms, including yeasts (Pebernard *et al.* 2006), *Drosophila melanogaster* (Li *et al.* 2013), Caenorhabditis *elegans* (Toraason *et al.* 2022), *Arabidopsis thaliana* (Li *et al.* 2019), and human (Guerineau *et al.* 2012). Smc5 and Smc6 are the 2 core components of the Smc5/6 complex and comprise of additional 6 known non-SMC elements (NSEs) proteins, which include Nse1, Nse2/Mms21, Nse3/MAGE-G1, Nse4, Nse5, and Nse6 (Pebernard *et al.* 2006; Liao *et al.* 2021; Serrano *et al.* 2020). It has been demonstrated that SMC5, SMC6, and NSE4 kleisin constitute the structural and functional core of this complex, where the interaction between SMC5/SMC6 and NSE1/NSE3 is mediated by NSE4 kleisin (Palecek *et al.* 2006; Aragón 2018; Odiba *et al.* 2022). In yeast, the N-terminal domain of the Nse4 kleisin directly interacts with the neck region of Smc6, linking it to the head region of Smc5, and the KITE proteins (Nse1 and Nse3) (Vondrova *et al.* 2020). Previous research in yeast has shown that Nse1 acts as a ubiquitin ligase involving a RING finger domain (Mokas *et al.* 2009), while Nse2/Mms21 has a SUMO ligase activity (Stephan, Kliszczak, *et al.* 2011; Stephan, Kliszczak, Morrison, *et al.* 2011). Interestingly, a recent study showed that Smc5/6 forms DNA loops through extrusion and reeling DNA symmetrically into loops at a rate of 1 kilobase pair per sec which is dependent on ATP hydrolysis. They further showed that Smc5/6 extrudes loops in the form of dimers and monomeric Smc5/6 unidirectionally translocates along DNA. However, Nse5/6 negatively regulates loop extrusion by hindering Smc5/6 dimerization, thus inhibiting the initiation of loop extrusion (Pradhan *et al.* 2023).

Among the Smc5/6 complex proteins, the role of Nse3 in chromosomal stability is not well characterized. Nse3 has a characteristic MAGE (Melanoma Antigen Genes) homology domain

Received on 26 May 2023; accepted on 17 July 2023

identified in several organisms, including yeast, plants, *C. elegans*, mice, and humans (Pebernard *et al.* 2004; Guerineau *et al.* 2012; Jeong *et al.* 2017; Li *et al.* 2019). While only a single MAGE gene exists in lower eukaryotes (Tacer *et al.* 2019; Florke Gee *et al.* 2020), the MAGE family broadens and diverges in evolutionarily advanced eukaryotes (eutherians), with humans containing more than 50 well-conserved MAGE genes (Lee and Potts 2017; Tacer *et al.* 2019; Florke Gee *et al.* 2020). MAGE proteins were initially classified based on their unique expression patterns. For instance, type I MAGEs are naturally expressed in spermatogonia but not in any other somatic tissue (Colemon *et al.* 2020). While many MAGE proteins, such as mouse Mageg2, are only expressed in reproductive tissues, they are aberrantly expressed in a wide range of cancer types (Weon and Potts 2015; Jeong *et al.* 2017). Notably, MAGE-C2-TRIM28 targets p53 for proteasome dependent degradation, in line with its tumor-promoting properties (Doyle *et al.* 2010), and MAGEC3 mutations have been linked to early-onset BRCA-negative ovarian cancers (Ellegate *et al.* 2022). Previous research in *A. thaliana* has shown that *AtNSE3* is required for embryogenesis and postembryonic development (Li *et al.* 2019), and *AtNSE3* expression is upregulated in response to double-strand breaks (DSBs) (Li *et al.* 2019).

Much of the current knowledge about MAGE proteins comes from single-cell-based analysis in yeast, and human cell lines, and from studies on *A. thaliana* (Pebernard *et al.* 2004, 2006; Guerineau *et al.* 2012; Li *et al.* 2019). In this study, we characterized the role of *mage-1* in *C. elegans*, a suitable animal system for studying DNA damage response (Gartner and Engebrecht 2022). Our results show that *mage-1* is involved in meiotic recombination and the repair of DNA lesions resulting from exposure to a range of genotoxic chemicals. We further show that NSE-1::GFP nuclear location depends on MAGE-1.

Materials and methods

Worm strains and maintenance

Worms were maintained at 20°C on nematode growth medium (NGM) plates with OP50 (*Escherichia coli* strain) as food source (Brenner 1974). All the strains were backcrossed with the wild type at least 4 times before use (Supplementary Table 1)

Construction of *mage-1* mutants by CRISPR/CAS9

Two *mage-1* mutants *mage-1*(*wsh2*) and *mage-1*(*wsh3*) were constructed by CRISPR/CAS9 method (Dickinson and Goldstein 2016). The *mage-1* sgRNA recognition site near to N-terminal of the *mage-1* gene from 277 to 296 was selected (Supplementary Table 12), and the pU6::mage-1 N-sgRNA template was constructed by fusion PCR (Ward 2014). Then, the pDD162, pCFJ90, and pCFJ104 plasmids, together with pU6::mage-1 N-sgRNA template, were microinjected into a young adult of N2. The F1 progeny expressing pCFJ90 and pCFJ104 plasmid were picked out under Olympus SZX2-ILLB fluorescence microscope and plated 1 worm per plate to lay eggs for 2 days. Worms were then picked for lysis and PCR screened using the primers indicated in Supplementary Table 12. The PCR products of mutants were sequenced for confirmation, and the *mage-1* mutants were backcrossed to N2 4 times before use.

Phenotypic assays

For the brood size analysis, 25 L4 hermaphrodites from each strain were placed on NGM plates with OP50 in the center (1 worm per plate). The worms were moved into freshly seeded NGM plates every 12 hours, and the total number of eggs laid on the previous plate was recorded. We repeated this process for each worm until egg-laying ceased, thereafter, the total number of fertilized eggs laid by each strain was analyzed. Hatched eggs were counted 24 hours after the eggs were laid, and the progeny viability was calculated as the proportion of hatched eggs to the brood size. After 72 hours, when the males were old enough to be recognized, we recorded the number of males and calculated the frequency as a proportion (%) of the living animals.

Genotoxic assays

No less than 50 L1/L4 stage nematodes were treated with different doses of genotoxic agents, including methyl methane sulfonate (MMS), hydroxyurea (HU) and cisplatin, and scored for viability (Craig *et al.* 2012; Kim and Colaiácovo 2015). For the MMS and cisplatin worm sensitivity assays, the nematodes were exposed to the indicated doses (as shown in the results) for 16 hours, whereas for the HU assay, the worms were treated for 20 hours. The worms were then allowed to recover for 72 hours for L1 worms and 24 hours for L4 stage worms before viability scoring was conducted as follows. We plated 5 adult worms on 1 NGM plate seeded with OP50 to lay eggs for 6 to 8 hours. Thereafter, the worms were removed, and the number of eggs laid was tallied for each plate. After 24 hours, the number of dead eggs was counted. The progeny viability was determined by the percentage of hatched eggs to the total number of eggs laid. We carried out each experiment in triplicate for 3 independent repeats.

Developmental assay with genotoxic treatment

As described (Craig *et al.* 2012; Kim and Colaiácovo 2015), L1 developmental assays were conducted on worms treated with MMS, cisplatin, and HU. M9 buffer was used to filter L1 worms through an 11-µm nylon net filter (Millipore) and treated in quadruplicate with the indicated DNA damage agents. For the MMS and cisplatin sensitivity assays, the worms were treated for 16 hours at different doses (as indicated in the results), while for HU L1, worms were treated for 20 hours. After treatment, the worms in each tube were washed with M9, distributed on NGM agar plates seeded with OP50, and allowed to recover at 20°C for 48 hours. Thereafter, the developmental stages of the worms were analyzed using a stereo microscope. The experiment was performed in 3 independent repeats.

Yeast two-hybrid (Y2H) analysis

The yeast two-hybrid vectors were constructed including pGADT7-Nse-1, pGADT7-Mage-1 pGADT7-Nse-4, pGBKT7-Smc-5, pGBKT7-Smc-6, pGBKT7-Nse-1, pGBKT7-Mage-1, and pGBKT7-Nse-4. The *nse-4*, *smc-5*, *smc-6*, *nse-1*, and *mage-1* coding sequences were amplified from wild-type *C. elegans* cDNA by PCR using the primers indicated in Supplementary Table 12. For pGADT7-Nse-4 and pGBKT7-Nse-4 construction, the *nse-4* coding sequence was cloned into the pGBKT7 and pGADT7 vectors at the EcoRI and BamHI sites, respectively. For pGADT7-Nse-1 and pGBKT7-Nse-1 construction, *nse-1* coding sequence was cloned into pGBKT7 and pGADT7 vectors at the EcoRI and BamHI sites, respectively. For pGADT7-Mage-1 and pGBKT7-Mage-1 construction, the *mage-1* coding sequence was cloned into the pGADT7 and pGBKT7vectors at the XmaI and BamHI sites; for pGBKT7-Smc-5 construction, *smc-5* coding sequence was cloned into the pGBKT7 vector at the NcoI and PstI sites. For pGBKT7-Smc-6 construction, *smc-6* coding sequence was cloned into the pGBKT7 vector at the EcoRI site using ClonExpress II One Step Cloning Kit (Vazyme). The interactions between MAGE-1 and other SMC-5/6 complex subunits were studied using the Gal4-based yeast two-hybrid (Y2H) system. Each pairs of vectors

(pGADT7-Nse-1 and pGBKT7, pGADT7-Nse-1 and pGBKT7-Smc-5, pGADT7-Nse-1 and pGBKT7-Smc-6, pGADT7-Nse-1 and pGBKT7-Nse-1, pGADT7-Nse-1 and pGBKT7-Mage-1, pGADT7-Nse-1 and pGBKT7-Nse-4, pGADT7-Mage-1 and pGBKT7, pGADT7-Mage-1 and pGBKT7-Smc-5, pGADT7-Mage-1 and pGBKT7-Smc-6, pGADT7-Mage-1 and pGBKT7-Nse-1, pGADT7-Mage-1 and pGBKT7-Mage-1, pGADT7-Mage-1 and pGBKT7-Nse-4, pGADT7-Nse-4 and pGBKT7, pGADT7-Nse-4 and pGBKT7-Smc-5, pGADT7-Nse-4 and pGBKT7-Smc-6, pGADT7-Nse-4 and pGBKT7-Nse-1, pGADT7-Nse-4 and pGBKT7-Mage-1, pGADT7-Nse-4 and pGBKT7-Nse-4, pGADT7 and pGBKT7, pGADT7 and pGBKT7-Smc-5, pGADT7 and pGBKT7-Smc-6, pGADT7 and pGBKT7-Nse-1, pGADT7 and pGBKT7-Mage-1, pGADT7 and pGBKT7-Nse-4) for interaction analysis were co-transformed into the Y2H Gold strain, and transformants selection was performed on SD-Leu-Trp plates. Interaction tests on SD-Leu-Trp and SD-Leu-Trp-His plates (with 0, 1, 2, 5, or 10-mM 3-aminotriazole) were carried out at 30°C for 2–3 days. Three independent tests were conducted.

RNA extraction and RT-qPCR

RNA was extracted from 30 adult worms using the TransZol Up Plus RNA kit (TRAN) according to the manufacturer's instructions. Then cDNA was synthesized using HiScript III RT SurperMix for qPCR (Vazyme) according to the manufacturer's instructions. RT-qPCR was performed in a final volume of 20 µL containing 10 µL of 2xChamQ Universal SYBR qPCR Master Mix (Vazyme), 0.4 µL of 10-µM forward and reverse primers (Supplementary Table 12), 2.0 µL of cDNA, and 7.2 µL of sterile water. The real-time PCR was carried out as the following program: predegeneration at 95°C for 30 sec; 40 cycles of degeneration at 95°C for 10 sec, and extension at 60°C for 30 sec; and melting curve analysis for 1 cycle of at 95°C for 15 sec, 60°C for 60 sec, and 95°C for 15 sec. The $2^{-\triangle\triangle CT}$ method was applied to determine the relative expression levels of the tested genes by normalizing to the gamma tubulin (*tbg-1*) (Livak and Schmittgen 2001).

mage-1::gfp::3×flag strain construction

The *mage-1*::*gfp*::3×*flag* strain was constructed by CRISPR/CAS9 method (Dickinson and Goldstein 2016), to label the MAGE-1 with GFP at the C-terminal (Supplementary Table 12). The *mage-1* sgRNA recognition site was selected near to the stop codon of the *mage-1* gene, and the pU6::mage-1 sgRNA was constructed by fusion PCR (Ward 2014). The *mage-1*:: *gfp*::3×*flag* repair template was constructed by fusion PCR as follows: ∼500 bp upstream DNA sequence before the stop codon of *mage-1* gene was added before the start codon of the *gfp*:: 3×*flag* DNA fragment with a linker, and ∼500 bp downstream DNA sequence with the stop codon of *mage-1 gene* was added after the *gfp*:: 3×*flag* DNA fragment. The pDD162, pCFJ90, and pCFJ104 plasmids, together with pU6:: mage-1 sgRNA DNA fragment and *mage-1*::*gfp*:: 3×*flag* repair template, were microinjected into a young adult. pCFJ90 (P*myo*-2: mCherry:*unc-54* UTR) and pCFJ104 (P*myo*-3:mCherry:*unc-54* UTR) are both extra-chromosomal array markers, which express the mCherry reporter gene in the pharynx and the body wall muscle, respectively. The F1 progeny expressing pCFJ90 and pCFJ104 plasmid were picked out under Olympus SZX2-ILLB fluorescence microscope and plated 1 worm per plate to lay eggs for 2 days. Worms were thereafter picked for lysis and genotyped using the primers indicated in Supplementary Table 12. Following the isolation of the successful candidate, the strain was sequenced for confirmation, and backcrossed to N2 4 times before use.

Cytological analysis

The extraction, fixation, and immunostaining of germlines were carried out according to previously described procedure (Craig *et al.* 2012). All DAPI staining was done for 5 minutes with DAPI (100 ng/mL). For RAD-51 staining, after dissection and postfixation with formaldehyde, and acetone/methanol (50%/50%) for 10 minutes, and permeabilization by 3 × 10 minutes in PBST (0.3% Triton) at room temperature, the slides were washed 1 × 10 minutes in PBST (0.1% Tween), then pre-blocked with 2–3 drops of Image enhancer (Invitrogen) at room temperature for 20 minutes in a humid box. The slides were washed 3 × 10 minutes in PBST (0.1% Tween), blocked in PBST supplemented with 3% BSA for 30 minutes. Primary antibody Rabbit anti-RAD-51 and secondary antibody Goat Anti-Rabbit IgG (H + L) were used at 1/200 and 1/400 dilution, respectively. All images were acquired by a Zeiss LSM800 confocal microscope with Airyscan. Whole germline images were captured using 10× objective, and all other images were taken using a 63× objective with oil immersion. Z-stack pictures were used to score RAD-51 foci and DAPI-stained chromosomes.

Statistical analysis

To assess statistical significance when comparing datasets, we used 1-way ANOVA with Fisher's LSD, 2-way ANOVA with Dunnett's multiple comparisons, and 2-tailed χ^2 Fisher's exact test as described in the relevant figure legends. Asterisks indicated the confidence level, with $P > 0.05$ (ns), $^{*}P < 0.05$, $^{**}P < 0.01$, and $^{****}P < 0.0001$. The confidence level for the unpaired 2-tailed Student's *t*-test was set at $P > 0.05$ (ns), $^{*}P \leq 0.05$, and $^{**}P \leq 0.01$. Bars with error bars represent means ± SEM.

Results

Mutation of *mage-1* leads to reduced fertility and increased incidence of male

To investigate the function of *mage-1* in *C. elegans*, we generated *mage-1* frameshift mutations using the CRISPR-Cas9 method (Supplementary Fig. 1). The *mage-1*(*wsh2*) allele has 2-nucleotide replacement and a single-nucleotide insertion in exon 3, while *mage-1*(*wsh3*) has a 7-nucleotide deletion. Both mutations lead to a frameshift (Fig. 1a). *mage-1*(*wsh2*) and *mage-1*(*wsh3*) mutants have a significantly decreased brood size compared to the wild type (51 and 54%, respectively) (Fig. 1b); the brood size being slightly lower compared to *smc-5*(*ok2421*) and *smc-6*(*ok3294*) mutants. Similarly, progeny viability of *mage-1*(*wsh2*) and *mage-1*(*wsh3*) was also decreased by 24 and 28%, respectively (Fig. 1c). In addition, a slight but significant "high incidence of male" (him) phenotype (1.5%, $n = 2000$) was observed in the *mage-1*(*wsh2*) mutant (Fig. 1d), indicating possible defects in meiotic recombination and/or chromosome segregation.

mage-1 mutants exhibited increased RAD-51 accumulation

Errors in meiotic chromosome segregation can arise from defects in DSB repair (Liu and Kong 2021; Gartner and Engebrecht 2022). We, therefore, monitored the appearance and disappearance of the RAD-51 recombinase foci at DSB sites in the germline (García-Muse 2021). In wild-type RAD-51 foci characteristically begin to appear at the transition zone (TZ), where meiotic DSB are induced by the SPO-11 nuclease (Koury *et al.* 2018). The steady-state level of RAD-51 foci increases in early pachytene (EP), peaks at mid pachytene (MP), and gradually disappears in late pachytene (LP) (Koury *et al.* 2018; García-Muse 2021). In *mage-1* mutants, we detected a

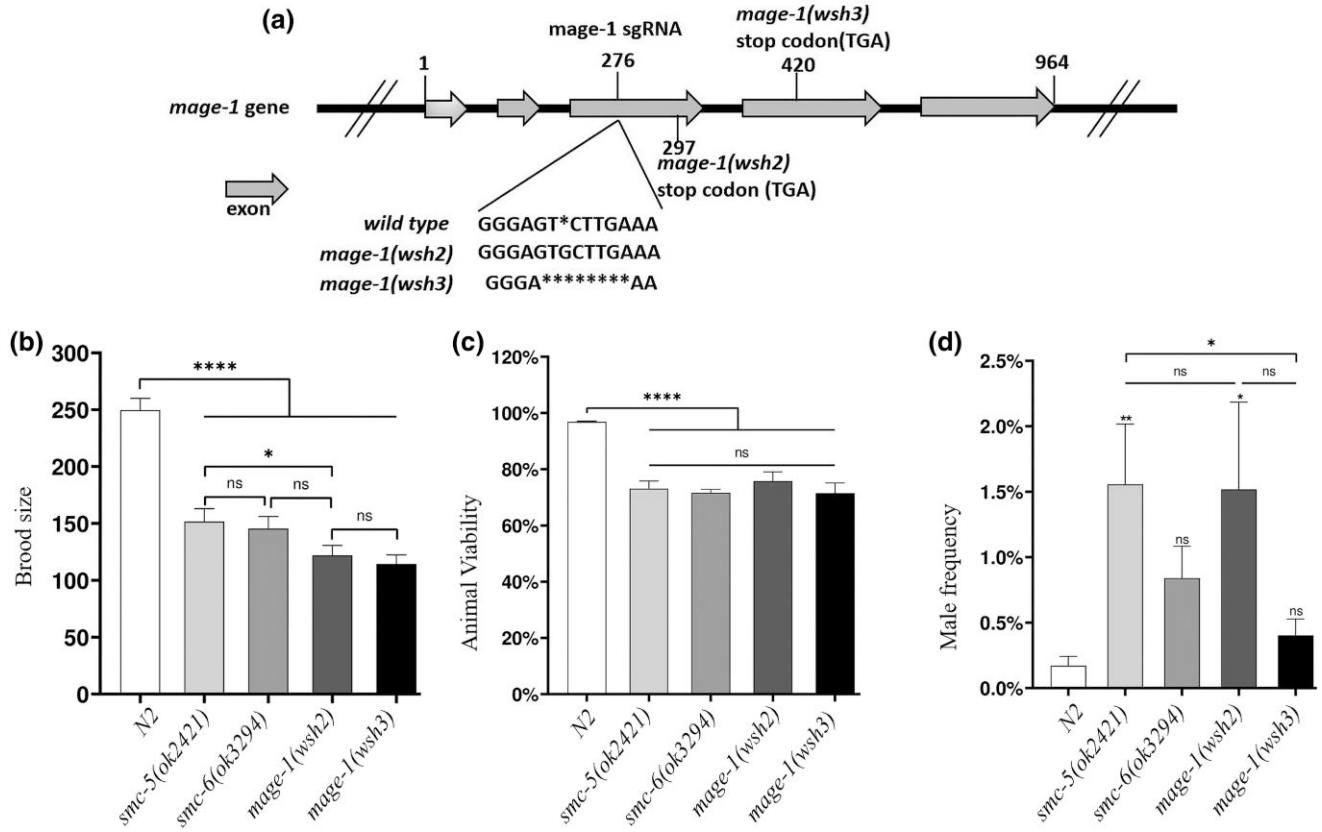

Fig. 1. Genotype and fecundity of *mage-1* mutants. a) Gene structures of *C. elegans mage-1*, and mutants generated by the CRISPR-Cas9 method. The *mage-1*(*wsh2*) mutant leads to G280A and T281A changes, and the insertion of a "G" after base 281, which results in a frameshift beginning from amino acid 63, and a stop codon at residue 68. In the *mage-1*(*wsh3*) mutant, bases 280 to 286 are deleted, resulting in a frameshift mutation beginning at residue 63 and a termination codon at residue 86. b) Brood size. c) Animal viability. d) Male frequency. Number of animals *n*; N2 = 24, *smc-5*(*ok2421*) = 21, *smc-6*(*ok3294*) = 20, *mage-1*(*wsh2*) = 21, *mage-1*(*wsh3*) = 22. Mutants were compared with N2 wild type using 1-way ANOVA with Fisher's LSD. $^{*}P < 0.05$, $^{**}P < 0.01$, $^{****}P < 0.0001$, and $P > 0.05$ (ns).

significantly increased number of RAD-51 foci in the mitotic region, as well as throughout the various stages of meiotic prophase (Fig. 2a–d and Supplementary Table 2). Most notable, a high number of RAD-51 foci persist in late pachytene, a stage where foci are largely gone in the wild type. To differentiate physiological DSBs from damage-induced DSBs, we crossed the *mage-1* mutants to *spo-11* mutant and analyzed RAD-51 distribution. Our result showed a lot of RAD-51 foci that persisted throughout the germline of the *mage-1*; *spo-11* double mutants when compared to the wild type and to the *spo-11* single mutant (with almost no RAD-51 foci) (Fig. 2a and e–g and Supplementary Table 2). However, the number of foci was reduced in *mage-1*; *spo-11* compared to *mage-1*. The significant increase of RAD-51 foci in *mage-1*; *spo-11* in the premeiotic zone points to persistent DSBs that may have originated from replication-induced DSBs (Wolters *et al.* 2014). The pattern of RAD-51 foci observed in the *mage-1* mutants tallies with previous reports on RAD-51 distribution in *smc-5*(*ok2421*) and *smc-6*(*ok3294*) mutants (Hong *et al.* 2016). The increased number of RAD-51 foci in mitotic cells, as well as meiotic cells, indicates a role of MAGE-1 in mitotic and meiotic DSB repair.

mage-1 deficiency leads to the formation of SPO-11-independent DSBs and affects accurate inter-sister recombinational repair

Defects in meiotic DSB repair can result in abnormal chromosome morphology (O'Neil *et al.* 2013). We examined chromosome morphology by monitoring DAPI-stained chromosomes in -1 and -2 diakinesis oocytes. Whereas 6 bivalents are present in the wild type as revealed by 6 compact DAPI-stained bodies, more than 30% of *mage-1* oocytes contained chromosome fragments (Fig. 3a and b). This outcome is similar to the number of chromosome fragments in the diakinesis oocytes of worms lacking SMC-5 (Wolters *et al.* 2014). Bickel *et al.* (2010) showed that chromosome fragments were present in *smc-5*; *spo-11* double mutant, confirming that the DSBs were SPO-11 independent. Likewise, we quantified the number of nuclei with chromosome fragments in the -1 and -2 diakinesis nuclei in the *mage-1*; *spo-11* double mutants, and observed a high number of diakinesis nuclei with fragments that did not change significantly when compared to the *mage-1* single mutants (Fig. 3a and b). This suggests that the chromosome fragments in the *mage-1* single mutants resulted from SPO-11-independent DSBs. Importantly, while RAD-51 foci were significantly reduced in the *smc-5*; *spo-11* strain compared to *smc-5*, some foci and chromosome fragments remained (Bickel *et al.* 2010). Intriguingly, the number of RAD-51 foci and oocytes with fragments in *mage-1*; *spo-11* closely resembled that of *mage-1*. This indicates that MAGE-1 deficiency leads to greater DNA damage accumulation than SMC-5 deficiency.

In *C. elegans*, typically only 1 DSB is designated for crossover (CO) per chromosome pair, despite several SPO-11 dependent DSBs being created (Altendorfer *et al.* 2020). Excess DSBs that are not resolved as COs or as nCOs via the inter-homolog recombination mechanism are repaired using the sister chromatid as a

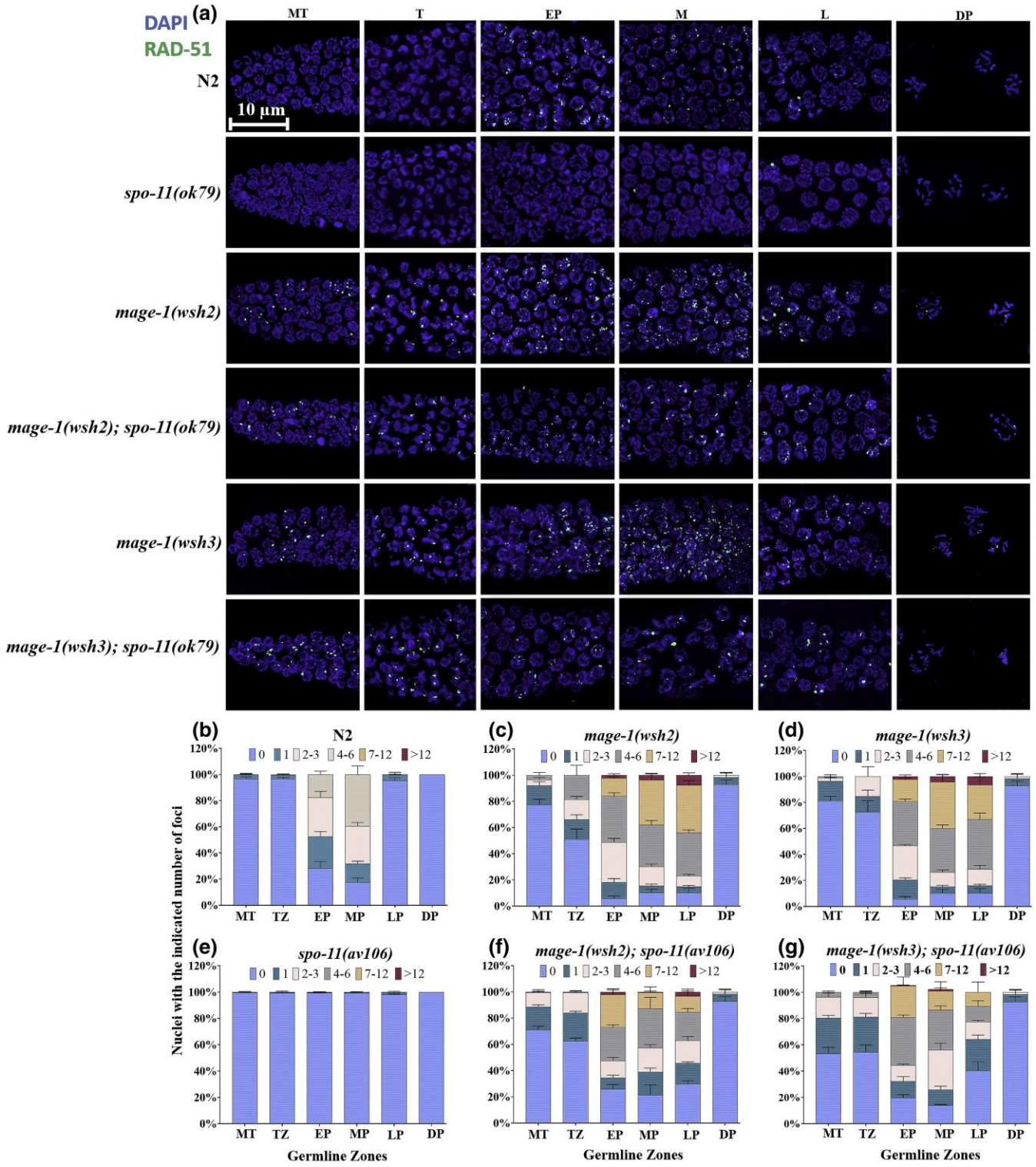

Fig. 2. RAD-51 accumulation in the mitotic and meiotic germ cells of *mage-1* mutants. a) Micrographs of max-projected images of RAD-51 foci and DAPI-stained nuclei. b–g) Quantification of RAD-51 foci in the germline, shown as the average number of foci per nucleus in each zone. Error bars represent standard error (±SEM). Twelve (12) gonads were scored per genotype. Images were captured using a Zeiss LSM 800 confocal microscope with Airyscan using a 63× objective (scale bar = 10 µm).

template (Adamo *et al.* 2008). When synaptonemal complex formation is disrupted, such as in the *syp-2* mutant, additional mutation in *brc-1* leads to defective inter-sister repair, resulting in the formation of chromosomal fragments that are visible in diakinesis nuclei (Adamo *et al.* 2008). About 98% of the *syp-2*(*ok307*) single mutants exhibited 12 univalents in the diakinesis oocytes, while 37% of diakinesis nuclei in *mage-1*(*wsh2*); *syp-2*(*ok307*) and *mage-1*(*wsh3*); *syp-2*(*ok307*) double mutants showed more than 12 DAPI-stained bodies (Fig. 3a and b). Remarkably, the average number of fragmented pieces are significantly less in the *mage-1*; *spo-11*

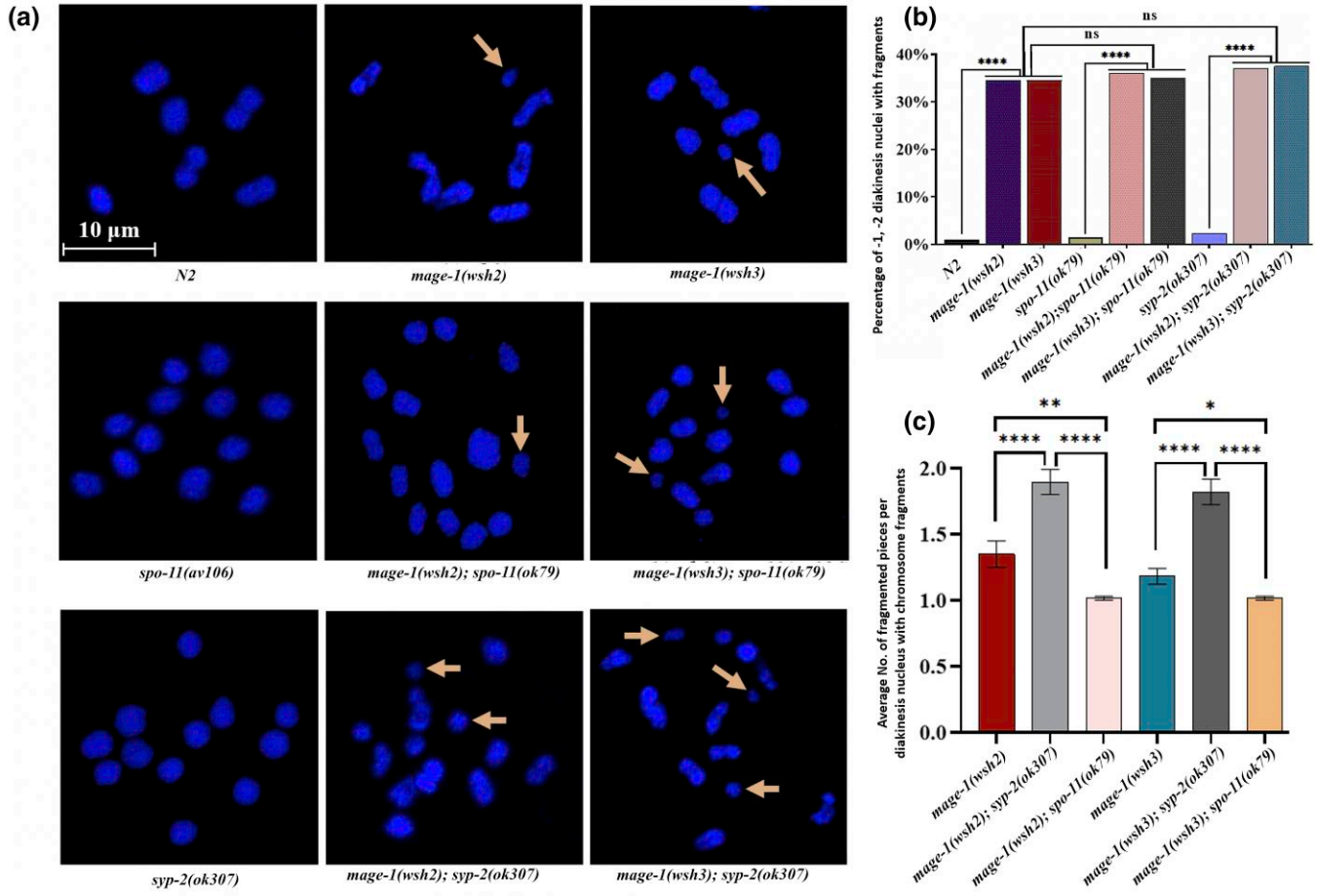

Fig. 3. Chromosome fragments in the *mage-1* mutants are linked to defects in inter-sister repair. a) Representative micrographs of diakinesis chromosomes in the single and double mutants. Arrows point to chromosome fragments. b) Quantification of chromosomes in -1 and -2 diakinesis nuclei of the *mage-1* single mutants showed a significantly higher number of fragmentations than the wild type (****$P < 0.0001$, χ^2 Fisher's exact test, $n = 250$ for each genotype). Similarly, the number of fragments in the *mage-1*; *spo-11* double mutants was significantly higher than the number recorded for *spo-11* single mutant (****$P < 0.0001$, χ^2 Fisher's exact test, $n = 250$ for each genotype). Likewise, the number of fragments found in the *mage-1*; *syp-2* double mutants is significantly higher than that found in the *syp-2* single mutant (****$P < 0.0001$, χ^2 Fisher's exact test, $n = 250$ for each genotype). Remarkably, there was no significant difference between the amount of fragments in the *mage-1* single mutant, *mage-1*; *spo-11*, and *mage-1*; *syp-2* double mutants ($^{ns}P > 0.05$, χ^2 Fisher's exact test, $n = 250$ for each genotype). Scoring of diakinesis nuclei and image capturing was carried out using a Zeiss confocal microscope LSM 800 with Airyscan using a 63× objective (scale bar = 10 µm).

double mutants, but more in the *mage-1*; *syp-2* double mutants compared to *mage-1* single mutants (Fig. 3c), suggesting that MAGE-1 is involved in inter-sister recombinational repair of meiotic DSBs.

The defect in the repair of meiotic DSBs as observed by defective RAD-51 distribution and diakinesis chromosome fragmentation prompted us to check for changes in CO designation (Adamo *et al.* 2008; Rosu *et al.* 2011). CO-designated sites are marked by COSA-1 foci in late pachytene cells (Yokoo *et al.* 2012; Ezechukwu *et al.* 2022; Haversat *et al.* 2022). We found that *mage-1* mutants contained 6 COSA-1 foci, 1 for each chromosome, as is the case for wild type (Supplementary Fig. 2).

mage-1 mutants are hypersensitive to MMS, HU, and cisplatin

To obtain further evidence for the role of MAGE-1 in DNA repair, we treated *mage-1* mutants with different types of DNA damage agents, including MMS, HU, and cisplatin (Craig *et al.* 2012). We aimed to find clues to the DNA damage repair pathways in which *mage-1* might be involved. By focusing on the major repair pathways, we included mutants that have been previously identified in various DSB repair pathways, including checkpoint (*clk-2*) (Ahmed *et al.* 2001), homologous recombination (*mus-81* and *xpf-1*) (Saito *et al.* 2009; Agostinho *et al.* 2013; O'Neil *et al.* 2013; Sabatella *et al.* 2021), inter-sister repair (*brc-1*) (Adamo *et al.* 2008), nonhomologous end joining (*lig-4*) (Clejan *et al.* 2006; Vujin *et al.* 2020), and translesion synthesis (*polh-1*) (Kim and Michael 2008). Comparing the phenotypes of the *mage-1* mutants with those mutants provides positive controls. *mage-1* worms (L4 stage) treated with MMS, (which impairs replication fork progression by DNA alkylation), showed reduced progeny viability compared to the wild type (Fig. 4a and Supplementary Table 3). This result is consistent with previous findings that Smc5/6 is needed to keep stalled replication forks in a stable, recombination-competent state to restart replication (Irmisch *et al.* 2009). We also treated *mage-1* worms (L1 stage) with 0.15 and 0.4-mM MMS which resulted in 100% sterility, while being largely unaffected in the N2 wild type (Fig. 4b and Supplementary Table 4). To further understand the reason for the sterility, we treated the worm with 0.15-mM MMS and viewed the worms under the microscope. Our result showed that the MMS-treated *mage-1* mutants did not develop a healthy germline (Supplementary Fig. 3). HU is an inhibitor of ribonucleotide reductase and induces DNA replication stress by depleting dNTP pools (Wozniak and Simmons 2021). In contrast to MMS treatment, HU treatment (L1 stage) did not lead to a dose-dependent decrease in the progeny viability of *mage-1* mutants (Fig. 4c and Supplementary Table 5). Cisplatin treatment induces base damage and DNA intra and interstrand crosslinks (ICLs) (Lemaire *et al.* 1991; Meier *et al.* 2014). *mage-1*(*wsh2*) and *mage-1*(*wsh3*) mutants treated with 50-mM cisplatin at the L4 stage showed significantly decreased progeny viability (50 and 20%, respectively) compared to wild type (95%) (Fig. 4d and Supplementary Table 6). Treatment at 200- and 400-mM doses of cisplatin led to non-survival of the vast majority of *mage-1*(*wsh2*) and *mage-1*(*wsh3*) progeny, with the wild type largely surviving (Fig. 4d and Supplementary Table 6). Overall, *mage-1* appears to play important roles in the repair of stalled replication fork and DNA intra and interstrand crosslinks through homologous recombination.

DNA damage signaling can induce a transient cell cycle arrest in the mitotic zone of *C. elegans* germ cells, which manifests as a reduced steady-state level of mitotic cells, with cells being enlarged due to their continued growth in the absence of cell division (Ahmed *et al.* 2001). DAPI staining of the germlines from both *mage-1* mutants treated with 50-mM cisplatin revealed the presence of hyper-enlarged mitotic nuclei, with cell numbers being lower at all stages compared with the wild type (Fig. 4e). Furthermore, there were chromosome fragments present in the diakinesis oocytes of the *mage-1* mutants. Altogether, these data indicate that MAGE-1 is not required for DNA damage checkpoint signaling but is essential for repairing chemically-induced DNA damage in the *C. elegans* germline.

Defective DNA repair in somatic cells may cause developmental delay or arrest, as well as the early death of larvae (Craig *et al.* 2012; Vermezovic *et al.* 2012). To investigate the influence of the *mage-1* mutation on development, we exposed L1-stage worms to different sources of DNA damage. We employed the same set of control strains to provide additional clues on the pathways *mage-1* may be involved. We observed that the development of *mage-1* mutants is delayed compared to the wild type upon treatment with MMS (Fig. 5a–c and Supplementary Table 7), HU (Fig. 5d–g and Supplementary Table 8), and cisplatin (Fig. 5h–k and Supplementary Table 9). Generally, the developmental delay in the *mage-1* mutants was significant compared to N2 and similar to that of the *smc-5* and *smc-6* mutants, which is expected given that they are part of the same complex. However, notable differences were observed between *mage-1* mutants and the positive control strains. After MMS treatment, *clk-2* showed a more severe delay than the Smc5/6 mutants, while *mus-81* was similar. HU treatment resulted in a more pronounced delay in *clk-2* than in the Smc-5/6 mutants, while *polh-1* exhibited a lower delay. Cisplatin caused severe delay in the Smc-5/6 mutants, and worse in *xpf-1* mutants, but less in *brc-1* and *lig-4* mutants.

mage-1 mutants showed increased germ cell apoptosis

When cells fail to repair the damaged DNA, the cell death pathway will be activated, leading to the formation of apoptotic cells (Gartner *et al.* 2000). CEP-1/p53 is a well-characterized transcription factor in DNA damage response pathway in the *C. elegans* hermaphrodite germline and acts through the transcriptional activation of 2 pro-apoptotic genes, namely, *egl-1* and *ced-13* (Lane and Crawford 1979; Harris and Hollstein 1993; Schumacher *et al.* 2005; Conradt *et al.* 2016). To investigate whether the defect in the *mage-1* mutants could lead to increased apoptosis, we counted the number of apoptotic corpses marked by CED-1::GFP using fluorescence microscopy. CED-1 is a transmembrane protein expressed in engulfing (sheath) cells and clusters around cell corpses (Zhou *et al.* 2001). We observed significantly elevated levels of germ cell apoptosis in *mage-1*(*wsh2*) and *mage-1*(*wsh3*) mutants, with and without treatment with 50-μM cisplatin (Fig. 6a and b).

egl-1 is transcriptionally induced in cells destined to die, and EGL-1 protein triggers apoptosis by inhibiting the cell death protective function of CED-9, leading to the CED-4 dependent activation of the CED-3 caspase to trigger apoptosis induction (Schumacher *et al.* 2005; Conradt *et al.* 2016). In response to DNA damage, *C. elegans egl-1* and the *ced-13* paralog are transcriptionally induced by p53/CEP-1 (Greiss *et al.* 2008). We quantified the relative expression levels of *ced-13* and *egl-1* in the *mage-1* mutants using qRT-PCR (Fig. 6c and d). We included control strains representing different repair pathways in this assay to validate our findings from the DNA damage assay, which suggested the involvement of *mage-1* in DSB repair through the HR pathway and inter-sister repair. The *xpf-1*(*tm2842*), which is defective in repair and in resolving meiotic recombination intermediates (Schvarzstein *et al.* 2014; Jagut *et al.* 2016), exhibited a similar level

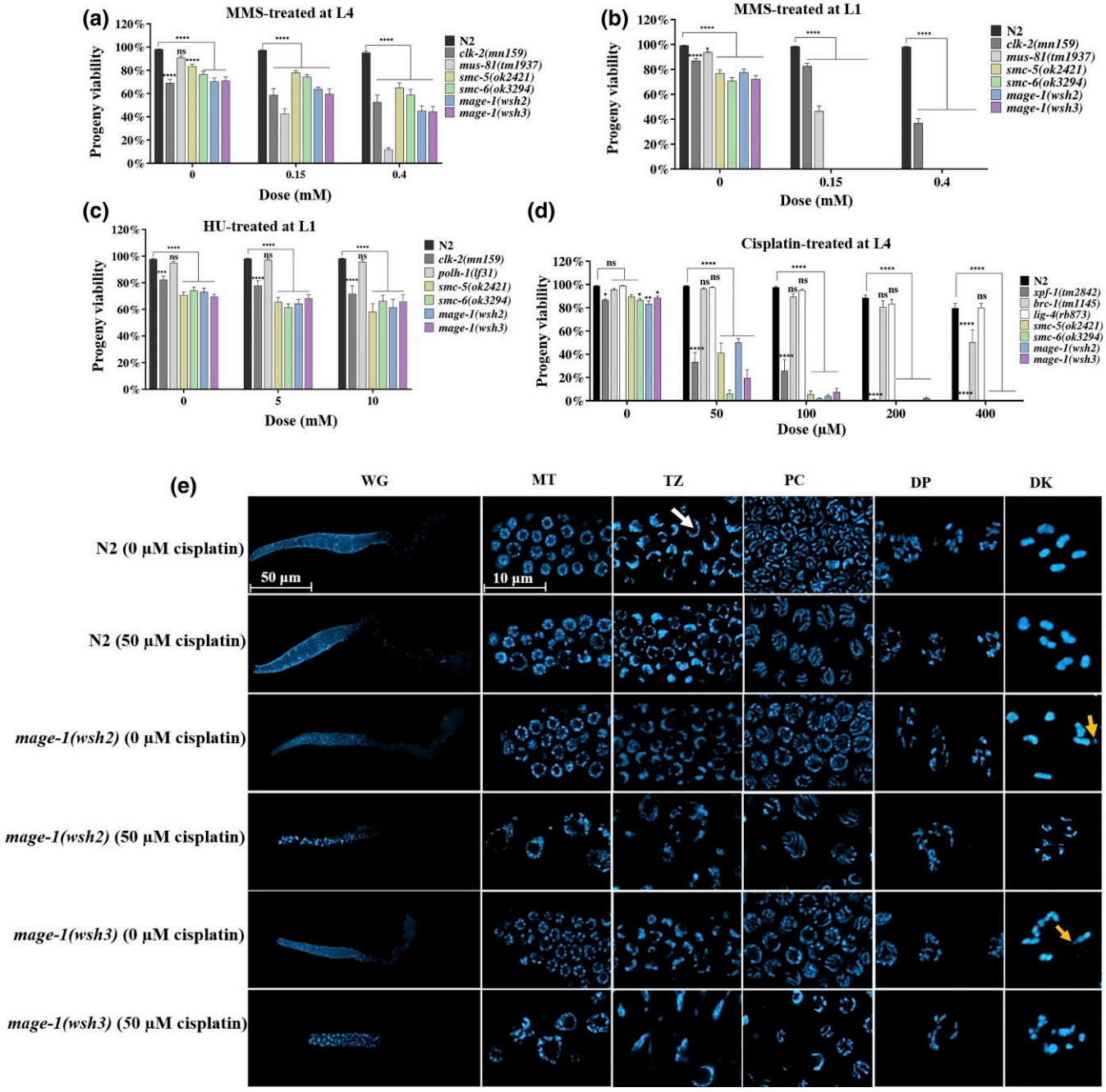

Fig. 4. Progeny viability of *mage-1* mutants treated with different genotoxic agents. a) MMS treatment at the L4 stage. b) MMS of L1 larvae. c) HU treatment at the L1 stage. d) Cisplatin treatment at L4 stage. The bar graphs show the mean ± SEM of worm viability compared to wild type (ns, not significant; $^{*}P < 0.05$; $^{**}P < 0.01$; $^{****}P < 0.0001$, 2-way ANOVA with Dunnett's multiple comparisons test. Number of animals *n* is represented in Supplementary Tables 3–6). Experiments were performed in 3 independent trials. e) Micrograph of DAPI-stained germline from cisplatin-treated at L4 stage. The arrow in the TZ points to a crescent-shaped nucleus typical of the transition zone, and the arrows in DK zones point to chromosome fragments. Whole germline pictures were captured using a Zeiss LSM 800 confocal microscope with a 10× objective (scale bar = 50 µm); the other images were captured with a 63× objective (scale bar = 10 µm). WG, whole germline; MZ, mitotic zone; TZ, transition zone; PC, pachytene; DP, diplotene; DK, diakinesis.

of *ced-13* and *egl-1* induction. *brc-1*(*tm1145*) mutants deficient in inter-sister repair showed increased levels of *ced-13* and *egl-1* induction compared to wild type but lower than the Smc5/6 complex mutants. In contrast, *lig-4*(*rb873*), which is defective in nonhomologous end joining (NHEJ), did not show increased *ced-13* and *egl-1* expression levels compared to the wild type. We found that *ced-13* and *egl-1* are induced in *mage-1* as well as in *smc-5* and *smc-6* mutants, to a level that exceeds cisplatin-treated wild-type worms (Fig. 6c and d; Supplementary Tables 10 and 11, respectively). When treated with cisplatin, *ced-13* and *egl-1* expression levels in *mage-1* mutants were further increased (Fig. 6c and d; Supplementary Tables 10 and 11, respectively). The increase of *egl-1* and *ced-13* expression levels in the *mage-1* mutants is likely due to unrepaired DSBs resulting from compromised meiotic recombination. Taken together, our results indicated that the *mage-1* mutations led to increased apoptosis.

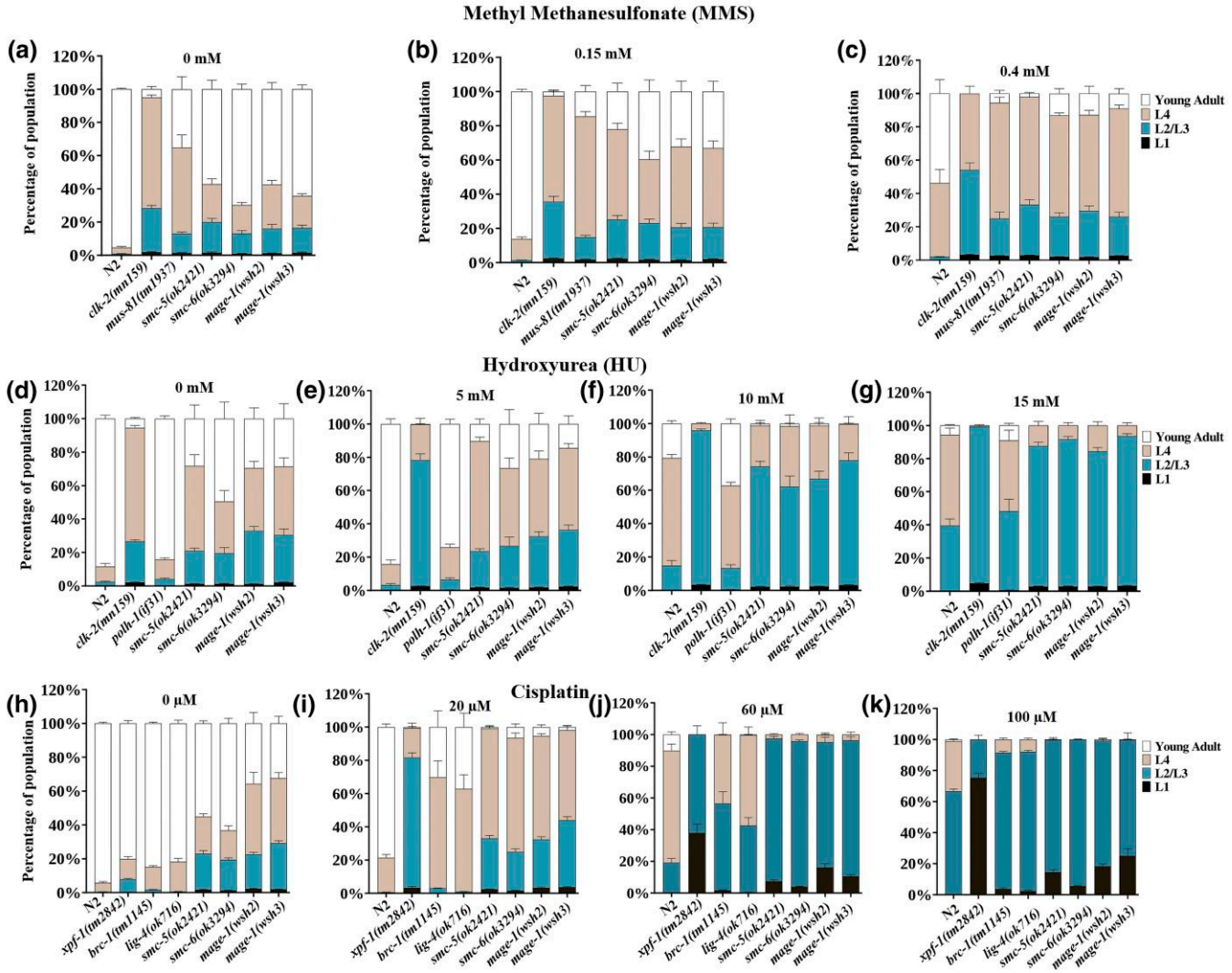

Fig. 5. Delayed development of *mage-1* mutants exposed to genotoxic agents. The proportion of worms in various developmental stages is shown. a–c) MMS treatment, d–g) HU treatment, and h and i) cisplatin treatment. The number of animals *n* is represented in Supplementary Tables 7–9. Experiment was performed in 3 independent trials.

NSE-1 steady-state levels are reduced in *mage-1* mutants

Previous studies in fission yeast have shown that Nse3 interacts with Nse1 and Nse4 within the Smc5/6 complex (Fig. 7a) (Zabrady *et al.* 2016). To investigate whether this interaction is conserved in *C. elegans*, we characterized the interaction of MAGE-1 with other members of the SMC-5/6 complex in *C. elegans* using the Y2H system. MAGE-1 only interacted directly with NSE-1 and NSE-4 subunits, but not with SMC-5 and SMC-6 (Fig. 7b). The interaction between MAGE-1, NSE-1, and NSE-4 was further confirmed by the presence of the 3 proteins when 6His-MAGE-1 was immunoprecipitated from whole *E. coli* cell lysates that co-expressed MAGE-1, NSE-1 and, NSE-4 proteins (Supplementary Fig. 4a), and western blot analysis of His and NSE-1 antibodies (Supplementary Fig. 4b). We also found that NSE-4 was able to interact with SMC-5, NSE-1, MAGE-1, and itself, but not with SMC-6 in the yeast two-hybrid assay (Fig. 7b).

Furthermore, we were interested in investigating the localization of MAGE-1, and hence used the CRISPR-Cas9 system to generate the *mage-1*::*gfp* transgenic strain. We found that MAGE-1 is associated with chromosomes (Fig. 7c). Since NSE-4 is a core component for stabilizing the SMC-5/6 complex and interacts with MAGE-1, we thought that the absence of NSE-4 will affect MAGE-1 distribution. Hence, we generated the strain *mage-1*::*GFP;nse-4*(*tm7158*) and examined the localization of MAGE-1::GFP. Our result showed that NSE-4 is required for the recruitment of MAGE-1 as the MAGE-1::GFP intensity was severely decreased in the *nse-4*(*tm7158*) background, and also displayed cytoplasmic localization in contrast to the wild type which exhibited chromosomal localization (Fig. 7c). Since MAGE-1 interacted directly with NSE-1, we also sought to examine whether mutation of *mage-1* would affect the localization of NSE-1. We had previously generated a *nse-1*::*gfp* knock-in strain by CRISPR-Cas9 (Odiba *et al.* 2022). In the wild type, NSE-1 localizes to the nucleus throughout all stages of germ cell development, with NSE-1 localization to distinct chromosomes becoming evident from the pachytene stage onwards (Fig. 7d) (Odiba *et al.* 2022). In contrast, the intensity of the NSE-1::GFP signal was dramatically decreased and hardly detectable in *mage-1* mutants (Fig. 7d). When the laser power was increased, we found a residual NSE-1::GFP signal associated with

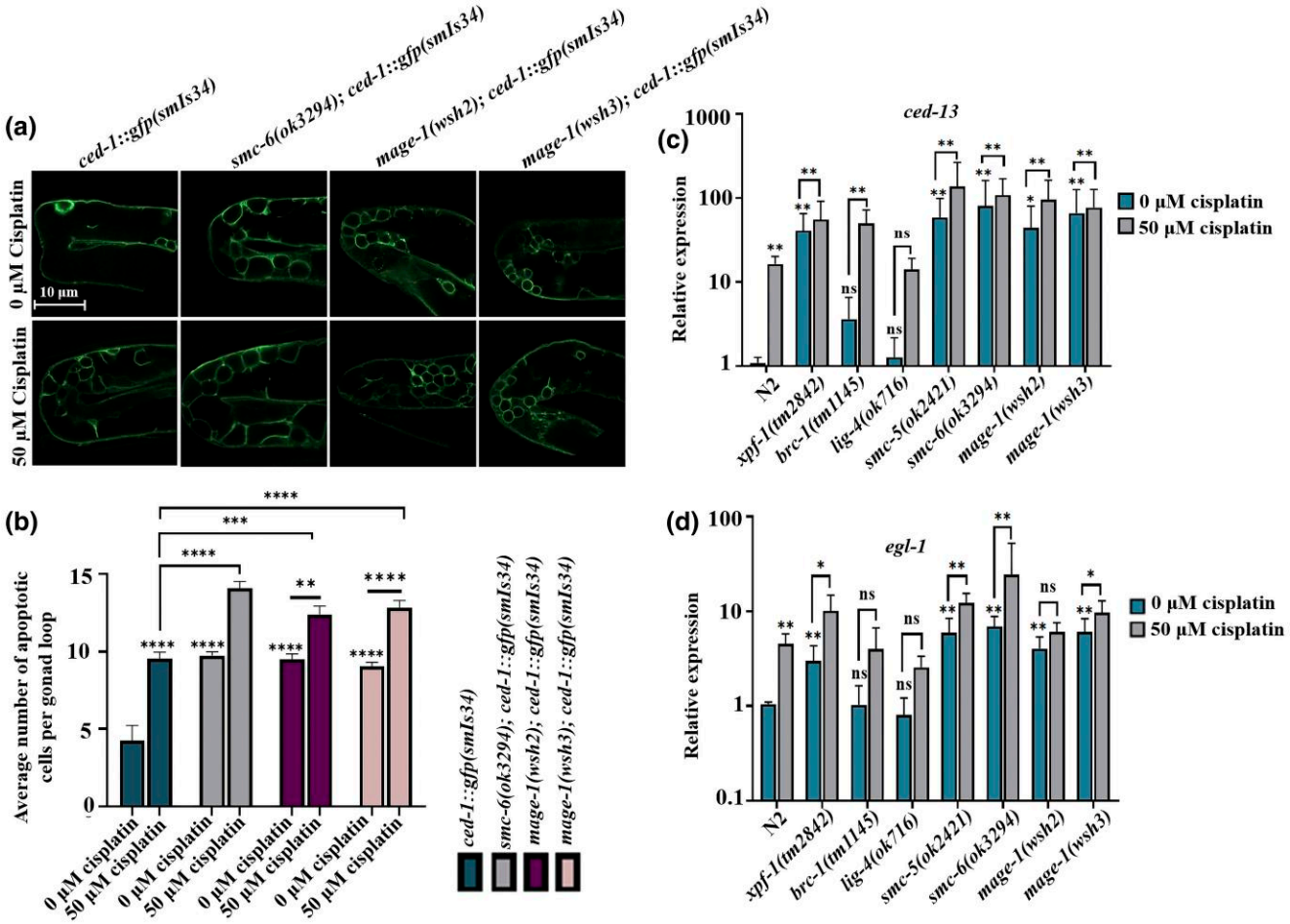

Fig. 6. Loss of *mage-1* leads to increased apoptosis in the *C. elegans* germline. a) Cell corpses were scored by apoptotic cells being surrounded by CED-1::GFP rings. b) Quantification of cell corpses showed that the number of apoptotic cells significantly (****$P < 0.0001$) increased in *smc-6(ok3294)*, *mage-1(wsh2)*, and *mage-1(wsh3)* mutants when compared to wild type (1-way ANOVA with Tukey's multiple comparisons test, $n = 50$ per treatment). c) Relative mRNA expression levels for *ced-13* and d) *egl-1* in the wild-type and mutant genotypes as measured by quantitative RT-PCR. *xpf-1(tm2842)*, *brc-1(tm1145)*, and *lig-4(rb873)* mutants were used as control strains with HR, inter-sister HR, and NHEJ pathways being defective, respectively (for comparisons to wild type; unpaired 2-tailed Student's *t*-test, $^{**}P \leq 0.01$, $^{*}P \leq 0.05$ and ns—$P > 0.05$, for comparing cisplatin-treated stains compared to untreated strains of the same genotype; $^{\#\#}P \leq 0.01$, $^{\#}P \leq 0.05$, and ns—$P > 0.05$). Experiments were performed in triplicate with 2 independent repeats. Zeiss confocal microscope LSM 800 with Airyscan using a 63× objective (scale bar = 10 µm) was used for scoring of oocytes and image capture.

chromosomes in early and middle pachytene cells of *mage-1(wsh2)* (Fig. 7e and Supplementary Fig. 5), the NSE-1::GFP signal otherwise being diffuse and largely focused in the cytoplasm in diplotene and diakinesis cells, as observed in *smc-5(ok2421)* mutants (Fig. 7d and e) (Odiba *et al.* 2022). The *mage-1(wsh3)* mutant showed diffused NSE-1::GFP location within the cytoplasm and the nucleus (without residual chromosome association), while *smc-5* mutation led to the exclusion of NSE-1 from nuclei and a stronger cytoplasmic signal. Our results indicate that NSE-1::GFP stability and location might depend on MAGE-1, NSE-1 chromosomal location depending on the SMC-5/6 complex.

Discussion

Since *C. elegans* contains just 1 MAGE gene (*mage-1*) (López-Sánchez *et al.* 2007), our study, for the first time, sheds light on the function of MAGE in a whole animal system. The decreased brood size and progeny viability and the increased incidence of males in the *mage-1* mutants compared with the wild type indicate a defect in meiosis (Stamper *et al.* 2013). This phenotype is similar to the *nse-4* mutants we previously reported (Odiba *et al.* 2022). Similarly, in *A. thaliana*, the loss of function of AtNSE3 resulted in severe defects in early embryonic development (Li *et al.* 2019). Furthermore, apical meristem and hypophysis differentiation in the AtNSE3 and AtNSE1 mutants is defective (Li *et al.* 2019). While it has been shown that Smc5/6 proteins are required for *A. thaliana* and *Saccharomyces cerevisiae* viability, they are not essential in *Drosophila* under normal conditions (Li *et al.* 2013).

Our results also showed increased RAD-51 foci in all zones of the germ line, ranging from mitotic cells all the way to the late pachytene cells, in the *mage-1* mutants compared to the wild type. This result tallies with the amount of RAD-51 reported for HR defective mutants including *nse-4* (Yamaguchi-Iwai *et al.* 1999; Bailly *et al.* 2010; Lee *et al.* 2010; Altendorfer *et al.* 2020; Odiba *et al.* 2022). Our findings also showed that a large proportion of the DSBs (as indicated by the RAD-51 foci) is SPO-11 independent. The appearance of RAD-51 foci in the mitotic area is most likely due to DNA breaks that resulted from DNA replication stress. In a previous study, the dynamics of the Rad51 and gamma-H2AX foci were also abnormal after irradiation in chicken DT40 *Smc5* mutant cells due to DSB repair deficiency (Stephan, Kliszczak, *et al.* 2011). A high number of DNA DSBs were also

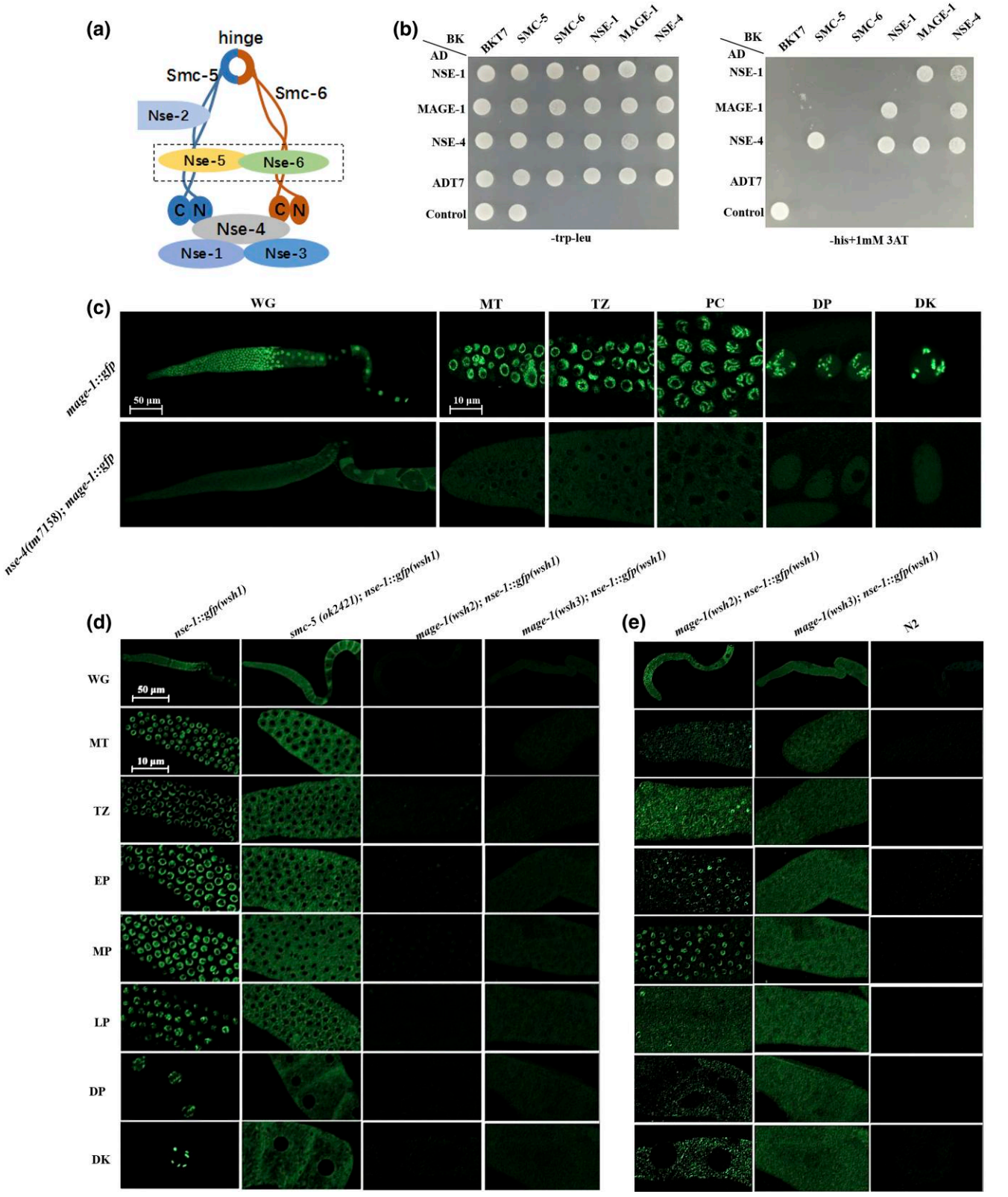

Fig. 7. MAGE-1 interacts with key members of the SMC-5/6 complex. a) Diagram of the fission yeast Smc5/6 complex. b) Yeast two-hybrid analysis of *C. elegans* Smc5/6 subunit interactions. c) MAGE-1 localizes to the chromosome in all zones of the germline and its distribution is affected by *nse-4*(*tm7158*) mutation, where MAGE-1::GFP signal sharply decreased in intensity and also localized in the cytoplasm d) NSE-1::GFP distribution in *mage-1* mutants. In the wild type, NSE-1 localizes to chromosomes throughout all stages of germ cell development. In the *smc-5* and *mage-1* mutants, NSE-1 was excluded from the nuclei throughout the germline. However, the intensity of the NSE-1::GFP signal was dramatically decreased and was hardly detected in the *mage-1* mutants. e) Images obtained with higher laser power show a zone-specific localization of NSE-1::GFP on the chromosomes in *mage-1*(*wsh2*) but not in *mage-1*(*wsh3*). All images for the whole germline were captured using a Zeiss LSM800 confocal microscope using a 10× objective (scale bar of 50 µm). All other images of the different zones were captured using a 63× objective (scale bar of 10 µm). WG, whole germline; MZ, mitotic zone; TZ, transition zone; EP, early pachytene; MP, mid pachytene; LP, late pachytene; DP, diplotene; DK, diakinesis.

reported to occur in the budding yeast *NSE3* and *NSE1* mutants (Li *et al.* 2017). Furthermore, errors in meiosis could be associated with faulty homologous recombination (HR), which leads to persistent DSBs and chromosome fragments that can be distinguished at diakinesis. Our findings show that a high number of diakinesis nuclei with chromosome fragments were SPO-11-independent. However, it is not clear at what stage this defect in DSB repair that accounted for these fragments occurred. The SMC5/6 complex works with cohesin to repair DSBs using sister chromatid recombination as a template in yeasts and human cells (Watanabe *et al.* 2009; Stephan, Kliszczak, *et al.* 2011). A previous report showed that chromosome mis-segregation and fragmentation occurred in *Schizosaccharomyces pombe Smc5/6* mutants (Irmisch *et al.* 2009). Similarly, the deletion of Smc5 in chicken DT40 cells increased the distances between sister chromatids in mitotic chromosomes, demonstrating that Smc5/6 regulates recombinational repair by ensuring proper sister chromatid cohesion (Stephan, Kliszczak, *et al.* 2011). The *mage-1* mutants were crossed with *syp-2(ok307)* to abrogate inter-homolog recombination (Colaiácovo *et al.* 2003; Adamo *et al.* 2008; Li *et al.* 2018), and extra chromosome fragments were observed in addition to the 12 DAPI staining bodies, indicating MAGE-1 contributed to the inter-sister recombination (Bickel *et al.* 2010). We have also observed this disruption of inter-sister recombination in *nse-4* mutants (Odiba *et al.* 2022), but the phenotype is milder compared to *mage-1*. Although a study suggested that the SMC5/6 complex is not crucial for premeiotic DNA replication and for meiosis in mouse spermatogenesis (Hwang *et al.* 2018), our result suggests that *mage-1* contributes to accurate inter-sister repair during meiosis in *C. elegans*.

The Smc5/6 complex has been implicated in various types of DNA repair, including DSBs, replication stress, and cross-link repair (Uhlmann 2016; Diaz and Pecinka 2018; Hwang *et al.* 2018; Serrano *et al.* 2020; Adamus *et al.* 2020; Toraason *et al.* 2022). In our study, the *mage-1* mutants were hypersensitive to MMS, HU, and cisplatin. *Smc5/6* mutants are hypersensitive to DNA damage in budding and fission yeast (Pebernard *et al.* 2004, 2006; Stephan, Kliszczak, Morrison, *et al.* 2011). In yeast, *Nse3* is involved in the homologous recombination repair of DNA damage and cellular resistance to a variety of genotoxic agents, and *NSE3* mutation in *S. pombe* results in hypersensitivity to DNA-damaging agents (Pebernard *et al.* 2004; Zabrady *et al.* 2016). In agreement, the expression of *AtNSE3* and *AtNSE1* was upregulated after DSB induction in *A. thaliana*, indicating that *AtNSE3* and *AtNSE1* play a role in DNA damage repair (Li *et al.* 2017). *D. melanogaster Smc5*, *Smc6*, and *MAGE* mutants were very sensitive to genotoxic agents such as camptothecin, MMS, hydroxyurea, and ionizing radiation (Taylor *et al.* 2008; Li *et al.* 2013). Likewise, the *Smc5* mutation in chicken DT40 cells was sensitive to MMS and ionizing radiation (IR), and irradiation resulted in increased chromosome aberrations (Stephan, Kliszczak, *et al.* 2011). Similarly, the SMC5/6 complex is needed for DNA repair in mice when exposed to exogenous DNA damage agents (Hwang *et al.* 2018).

Cell death was observed in the early stages of development in the NSE1 and NSE3 mutant embryos of *A. thaliana*, and cytological analysis further revealed that vacuolar programmed cell death and necrosis resulted in ovule abortion (Li *et al.* 2019). Our results showed an increased number of cell corpses in *mage-1* mutants (Fig. 6a and b), the number of corpses being further increased upon treatment with 50-μM cisplatin. It is likely that apoptosis eliminates cells with damaged chromosomes, consistent with the presence of chromosomal fragments, abnormally high numbers of RAD-51 foci, and the increased sensitivity to DNA-damaging agents in *mage-1* mutants. In the analysis of relative expression levels of *ced-13* and *egl-1*, our result shows that the fold ratio of *ced-13* induction is higher than that of *egl-1*. Overall, these results showed that the *mage-1* mutations led to more apoptosis, which depends on *ced-13* and *egl-1* induction the EGL-1 and CED-13. Apoptosis is also hyper-induced in *nse-4* mutants (Odiba *et al.* 2022).

The structure of Smc5/6 complex is highly conserved but vary across organisms including yeasts (Duan *et al.* 2009; Leung *et al.* 2011; Stephan, Kliszczak, *et al.* 2011; Zabrady *et al.* 2016; Lafuente-Barquero *et al.* 2017), plants (Díaz *et al.* 2019), flies (Li *et al.* 2013), and human cells (Serrano *et al.* 2020). For instance, in both budding yeast (*S. cerevisiae*) and fission yeast (*S. pombe*), Smc5 and Smc6 solely interact at the hinges, Nse2/Mms21 interacts with Smc5, and the Nse1-3-4 subcomplex interacts with the head region of Smc5 via Nse4 (Pebernard *et al.* 2004; Stephan, Kliszczak, *et al.* 2011; Guerineau *et al.* 2012; Diaz and Pecinka 2018; Serrano *et al.* 2020). Nse5-6 subcomplex interacts with the hinge region of Smc5 and Smc6 in budding yeast, and with the head region in fission yeast (Serrano *et al.* 2020). The interaction between Smc6 and the Nse1-3-4 subcomplex is another major distinction between the 2 yeasts (Duan *et al.* 2009; Stephan, Kliszczak, Morrison, *et al.* 2011). Two-hybrid assays showed no interaction between Nse1, Nse-3, or Nse-4 with Smc6 in the budding yeast (Palecek *et al.* 2006; Duan *et al.* 2009; Hudson *et al.* 2011). However, an interaction between Nse3/Nse4 and the Smc6 head was detected in fission yeast (Palecek *et al.* 2006; Duan *et al.* 2009; Hudson *et al.* 2011). Studies in insect cells did not find any interaction between Smc6 and the Nse1-3-4 subcomplex (Pebernard *et al.* 2004, 2006). Our results showed that MAGE-1 interacts directly with NSE-1 and NSE-4, while NSE-4 interacts directly with NSE-1, MAGE-1, SMC-5, and itself. In *A. thaliana*, NSE4 interacts with SMC5 but not with SMC6 (Palecek *et al.* 2006; Duan *et al.* 2009; Hudson *et al.* 2011), NSE1 interacts with NSE3 but not with NSE4, and NSE4 interacts with NSE3 and SMC5 (Diaz and Pecinka 2018; Díaz *et al.* 2019; Zelkowski *et al.* 2019). In the fruit fly *D. melanogaster*, Mage1 directly interacts with Nse4 and Nse1 (Li *et al.* 2013). Nonetheless, in humans, hNSE1 and hNSE4 are RING proteins to which MAGE-G1 binds (Diaz and Pecinka 2018; Adamus *et al.* 2020). We also found that the *mage-1(wsh3)* mutation affected the localization and distribution of NSE-1 in vivo, likewise, the *nse-4* mutation affected MAGE-1 distribution in vivo. In our previous work, we also found that NSE-4 localizes on the chromosome, and *nse-4* mutation delocalized NSE-1 from the chromosomes to the cytoplasm (Odiba *et al.* 2022). Previous studies showed that the loss of the components of the SMC5/6 complex, except for the SUMO ligase hMMS21/hNSE2, causes the degradation of other SMC5/6 complex members (Taylor *et al.* 2008). Numerous MAGEs bind to E3 RING ubiquitin ligases at the molecular level, controlling their subcellular localization, substrate specificity, and ligase activity (Feng *et al.* 2011; Florke Gee *et al.* 2020). The MAGEA1 WH/A and WH/B motifs bind to the TRIM31 coiled-coil domain to activate its ubiquitin-ligase activity (Kozakova *et al.* 2015). The NSE-1 in *C. elegans* contains a RING domain, which is predicted to be an E3 ligase. The ubiquitin activity of NSE-1 and its relationship with MAGE-1 is worthy of further investigation.

Overall, this study demonstrated the importance of the *C. elegans mage-1* in the maintenance of genome integrity and DNA repair, and provides additional insight into the architecture of the SMC-5/6 complex. Additionally, the presence of SPO-11 independent DSBs resulting from *mage-1* deficiency further strengthens the existing evidence supporting the role of the SMC-5/6 complex in suppressing replication stress.

Data availability

Strains and raw data from this study are available upon request. The authors confirm that all essential data supporting the results of the study are presented within the article, figures, and tables.

Supplemental material available at GENETICS online

Acknowledgments

We are grateful to Peng Wang for helping with microinjections.

Funding

This study was funded by the National Natural Science Foundation of China (31960129), the Guangxi Natural Science Foundation (2022GXNSFAA035435 and 2020GXNSFBA297093) and by Research Start-up Funding of the Guangxi Academy of Sciences (2017YJJ026). AG is supported by Korean taxpayers via the Korean Institute for Basic Science (IBS-R022-A2-2021). YH is supported by the National Natural Science Foundation of China (31900509) and the Programs of Shandong University Qilu Young Scholars. Some strains were provided by the CGC, which is funded by the NIH Office of Research Infrastructure Programs (P40 OD010440).

Conflicts of interest

The authors declare that there is no conflict of interest related to this study.

Literature cited

Adamo A, Montemauri P, Silva N, Ward JD, Boulton SJ, La Volpe A. BRC-1 acts in the inter-sister pathway of meiotic double-strand break repair. EMBO Rep. 2008;9(3):287–292. doi:10.1038/sj.embor.7401167.

Adamus M, Lelkes E, Potesil D, Ganji SR, Kolesar P, Zabrady K, Zdrahal Z, Palecek JJ. Molecular insights into the architecture of the human SMC5/6 complex. J Mol Biol. 2020;432(13):3820–3837. doi:10.1016/J.JMB.2020.04.024.

Agostinho A, Meier B, Sonneville R, Jagut M, Woglar A, Blow J, Jantsch V, Gartner A. Combinatorial regulation of meiotic holliday junction resolution in *C. elegans* by HIM-6 (BLM) helicase, SLX-4, and the SLX-1, MUS-81 and XPF-1 nucleases. PLoS Genet. 2013;9(7):e1003591. doi:10.1371/journal.pgen.1003591.

Ahmed S, Alpi A, Hengartner MO, Gartner A. *C. elegans* RAD-5/CLK-2 defines a new DNA damage checkpoint protein. Curr Biol. 2001;11(24):1934–1944. doi:10.1016/S0960-9822(01)00604-2.

Altendorfer E, Láscarez-Lagunas LI, Nadarajan S, Mathieson I, Colaiácovo MP. Crossover position drives chromosome remodeling for accurate meiotic chromosome segregation. Curr Biol. 2020;30(7):1329–1338.e7. doi:10.1016/j.cub.2020.01.079.

Aragón L. The Smc5/6 complex: new and old functions of the enigmatic long-distance relative. Annu Rev Genet. 2018;52(1):89–107. doi:10.1146/annurev-genet-120417-031353.

Bailly AP, Freeman A, Hall J, Déclais A-C, Alpi A, Lilley DMJ, Ahmed S, Gartner A. The *Caenorhabditis elegans* homolog of Gen1/Yen1 resolvases links DNA damage signaling to DNA double-strand break repair. PLoS Genet. 2010;6(7):e1001025. doi:10.1371/journal.pgen.1001025.

Bickel JS, Chen L, Hayward J, Yeap SL, Alkers AE, Chan RC. Structural maintenance of chromosomes (SMC) proteins promote homolog-independent recombination repair in meiosis crucial for germ cell genomic stability. PLoS Genet. 2010;6(7):e1001028. doi:10.1371/journal.pgen.1001028.

Brenner S. The genetics of *Caenorhabditis elegans*. Genetics. 1974;77(1):71–94. doi:10.1093/genetics/77.1.71.

Clejan I, Boerckel J, Ahmed S. Developmental modulation of nonhomologous end joining in *Caenorhabditis elegans*. Genetics. 2006;173(3):1301–1317. doi:10.1534/genetics.106.058628.

Colaiácovo MP, MacQueen AJ, Martinez-Perez E, McDonald K, Adamo A, La Volpe A, Villeneuve AM. Synaptonemal complex assembly in *C. elegans* is dispensable for loading strand-exchange proteins but critical for proper completion of recombination. Dev Cell. 2003;5(3):463–474. doi:10.1016/S1534-5807(03)00232-6.

Colemon A, Harris TM, Ramanathan S. DNA hypomethylation drives changes in MAGE-A gene expression resulting in alteration of proliferative status of cells. Genes Environ. 2020;42(1):1–13. doi:10.1186/s41021-020-00162-2.

Conradt B, Wu YC, Xue D. Programmed cell death during *Caenorhabditis elegans* development. Genetics. 2016;203(4):1533–1562. doi:10.1534/genetics.115.186247.

Craig AL, Moser SC, Bailly AP, Gartner A. Methods for studying the DNA damage response in the *Caenorhabditis elegans* germ line. In: Methods in Cell Biology. Vol. 107. 2nd ed. Cambridge (MA): Elsevier Inc.; 2012. p. 321–352. doi:10.1016/B978-0-12-394620-1.00011-4.

Díaz M, Pečinková P, Nowicka A, Baroux C, Sakamoto T, Gandha PY, Jeřábková H, Matsunaga S, Grossniklaus U, Pecinka A. The SMC5/6 complex subunit NSE4A is involved in DNA damage repair and seed development. Plant Cell. 2019;31(7):1579–1597. doi:10.1105/tpc.18.00043.

Diaz M, Pecinka A. Scaffolding for repair: understanding molecular functions of the SMC5/6 complex. Genes (Basel). 2018;9(1):36. doi:10.3390/genes9010036.

Dickinson DJ, Goldstein B. CRISPR-based methods for *Caenorhabditis elegans* genome engineering. Genetics. 2016;202(3):885–901. doi:10.1534/genetics.115.182162.

Doyle JM, Gao J, Wang J, Yang M, Potts PR. MAGE–RING protein complexes comprise a family of E3 ubiquitin ligases. Mol Cell. 2010;39(6):963–974. doi:10.1016/j.molcel.2010.08.029.

Duan X, Yang Y, Chen YH, Arenz J, Rangi GK, Zhao X, Ye H. Architecture of the Smc5/6 complex of *Saccharomyces cerevisiae* reveals a unique interaction between the Nse5-6 subcomplex and the hinge regions of Smc5 and Smc6. J Biol Chem. 2009;284(13):8507–8515. doi:10.1074/jbc.M809139200.

Ellegate J, Mastri M, Isenhart E, Krolewski JJ, Chatta G, Kauffman E, Moffitt M, Eng KH. Loss of MAGEC3 expression is associated with prognosis in advanced ovarian cancers. Cancers (Basel). 2022;14(3):731. doi:10.3390/cancers14030731/s1.

Ezechukwu CS, Odiba AS, Liao G, Fang W, Wang B. An endogenous mCherry-tagged COSA-1 as a crossover investigation tool in *Caenorhabditis elegans*. MicroPubl Biol. 2022;2022(eCollection 2022). doi:10.17912/micropub.biology.000627.

Feng Y, Gao J, Yang M. When MAGE meets RING: insights into biological functions of MAGE proteins. Protein Cell. 2011;2(1):7–12. doi:10.1007/S13238-011-1002-9.

Florke Gee RR, Chen H, Lee AK, Daly Christina A., Wilander BA, Fon Tacer K, Potts PR. Emerging roles of the MAGE protein family in stress response pathways. J Biol Chem. 2020;295(47):16121–16155. doi:10.1074/jbc.rev120.008029.

García-Muse T. Detection of DSBs in meiosis. Methods Mol Biol. 2021;2153:287–293. doi:10.1007/978-1-0716-0644-5_20.

Gartner A, Engebrecht J. DNA repair, recombination, and damage signaling. Genetics. 2022;220(2):iyab178. doi:10.1093/genetics/iyab178.

Gartner A, Milstein S, Ahmed S, Hodgkin J, Hengartner MO. A conserved checkpoint pathway mediates DNA damage-induced

apoptosis and cell cycle arrest in *C. elegans*. Mol Cell. 2000;5(3):435–443. doi:10.1016/S1097-2765(00)80438-4.

Golfier S, Quail T, Kimura H, Brugués J. Cohesin and condensin extrude DNA loops in a cell-cycle dependent manner. Elife. 2020;9(e53885):1–34. doi:10.7554/eLife.53885.

Greiss S, Schumacher B, Grandien K, Rothblatt J, Gartner A. Transcriptional profiling in *C. elegans* suggests DNA damage dependent apoptosis as an ancient function of the p53 family. BMC Genomics. 2008;9(1):334. doi:10.1186/1471-2164-9-334.

Guerineau M, Kriz Z, Kozakova L, Bednarova K, Janos P, Palecek J. Analysis of the Nse3/MAGE-binding domain of the Nse4/EID family proteins. PLoS One. 2012;7(4):e35813. doi:10.1371/journal.pone.0035813.

Hagstrom KA, Meyer BJ. Condensin and cohesin: more than chromosome compactor and glue. Nat Rev Genet. 2003;4(7):520–534. doi:10.1038/nrg1110.

Harris CC, Hollstein M. Clinical implications of the p53 tumor-suppressor gene. N Engl J Med. 1993;329(18):1318–1327. doi:10.1056/nejm199310283291807.

Haversat J, Woglar A, Klatt K, Akerib CC, Roberts V, Chen S-Y, Arur S, Villeneuve AM, Kim Y. Robust designation of meiotic crossover sites by CDK-2 through phosphorylation of the MutSγ complex. Proc Natl Acad Sci U S A. 2022;119(21):e2117865119. doi:10.1073/PNAS.2117865119.

Hong Y, Sonneville R, Agostinho A, Meier B, Wang B, Blow JJ, Gartner A. The SMC-5/6 complex and the HIM-6 (BLM) helicase synergistically promote meiotic recombination intermediate processing and chromosome maturation during *Caenorhabditis elegans* meiosis. PLoS Genet. 2016;12(3):e1005872. doi:10.1371/journal.pgen.1005872.

Hudson JJR, Bednarova K, Kozakova L, Liao C, Guerineau M, Colnaghi R, Vidot S, Marek J, Bathula SR, Lehmann AR, *et al.* Interactions between the Nse3 and Nse4 components of the SMC5-6 complex identify evolutionarily conserved interactions between MAGE and EID families. PLoS One. 2011;6(2):e17270. doi:10.1371/journal.pone.0017270.

Hwang G, Verver DE, Handel MA, Hamer G, Jordan PW. Depletion of SMC5/6 sensitizes male germ cells to DNA damage. Mol Biol Cell. 2018;29(25):3003–3016. doi:10.1091/mbc.E18-07-0459.

Irmisch A, Ampatzidou E, Mizuno K, O'Connell MJ, Murray JM. Smc5/6 maintains stalled replication forks in a recombination-competent conformation. EMBO J. 2009;28(2):144–155. doi:10.1038/emboj.2008.273.

Jagut M, Hamminger P, Woglar A, Millonigg S, Paulin L, Mikl M, Dello Stritto MR, Tang L, Habacher C, Tam A, *et al.* Separable roles for a *Caenorhabditis elegans* RMI1 homolog in promoting and antagonizing meiotic crossovers ensure faithful chromosome inheritance. PLoS Biol. 2016;14(3):e1002412. doi:10.1371/journal.pbio.1002412.

Jeong J, Jin S, Choi H, Kwon J, Kim J, Kim J, Park Z, Cho C. Characterization of MAGEG2 with testis-specific expression in mice. Asian J Androl. 2017;19(6):659–665. doi:10.4103/1008-682X.192033.

Kim HM, Colaiácovo M. DNA damage sensitivity assays in *Caenorhabditis elegans*. Bio Protoc. 2015;5(11):e1487. doi:10.21769/bioprotoc.1487.

Kim SH, Michael WM. Regulated proteolysis of DNA polymerase η during the DNA-damage response in *C. elegans*. Mol Cell. 2008;32(6):757–766. doi:10.1016/j.molcel.2008.11.016.

Koury E, Harrell K, Smolikove S. Differential RPA-1 and RAD-51 recruitment in vivo throughout the *C. elegans* germline, as revealed by laser microirradiation. Nucleic Acids Res. 2018;46(2):748–764. doi:10.1093/nar/gkx1243.

Kozakova L, Vondrova L, Stejskal K, Charalabous P, Kolesar P, Lehmann AR, Uldrijan S, Sanderson CM, Zdrahal Z, Palecek JJ. The melanoma-associated antigen 1 (MAGEA1) protein stimulates the E3 ubiquitin-ligase activity of trim31 within a TRIM31–MAGEA1–NSE4 complex. Cell Cycle. 2015;14(6):920–930. doi:10.1080/15384101.2014.1000112.

Lafuente-Barquero J, Luke-Glaser S, Graf M, Graf M, Silva S, Gómez-González B, Lockhart A, Lisby M, Aguilera A, Luke B. The Smc5/6 complex regulates the yeast Mph1 helicase at RNA-DNA hybrid-mediated DNA damage. PLoS Genet. 2017;13(12):e1007136. doi:10.1371/journal.pgen.1007136.

Lane DP, Crawford LV. T antigen is bound to a host protein in SY40-transformed cells. Nature. 1979;278(5701):261–263. doi:10.1038/278261a0.

Lee SJ, Gartner A, Hyun M, Ahn B, Koo HS. The *Caenorhabditis elegans* Werner syndrome protein functions upstream of ATR and ATM in response to DNA replication inhibition and double-strand DNA breaks. PLoS Genet. 2010;6(1):e1000801. doi:10.1371/journal.pgen.1000801.

Lee AK, Potts PR. A comprehensive guide to the MAGE family of ubiquitin ligases. J Mol Biol. 2017;429(8):1114–1142. doi:10.1016/j.jmb.2017.03.005.

Lemaire MA, Schwartz A, Rahmouni AR, Leng M. Interstrand cross-links are preferentially formed at the d(GC) sites in the reaction between cis-diamminedichloroplatinum (II) and DNA. Proc Natl Acad Sci U S A. 1991;88(5):1982–1985. doi:10.1073/pnas.88.5.1982.

Leung GP, Lee L, Schmidt TI, Shirahige K, Kobor MS. Rtt107 is required for recruitment of the SMC5/6 complex to DNA double strand breaks. J Biol Chem. 2011;286(29):26250–26257. doi:10.1074/jbc.M111.235200.

Li Q, Saito TT, Deshong AJ, Nadarajan S, Lawrence KS, Checchi PM, Colaiacovo MP, Engebrecht J. The tumor suppressor BRCA1/BARD1 complex localizes to the synaptonemal complex and regulates recombination under meiotic dysfunction in *Caenorhabditis elegans*. PLoS Genet. 2018;11(14):e1007701. doi:10.1371/journal.pgen.1007701.

Li X, Zhuo R, Tiong S, Di Cara F, King-Jones K, Hughes SC, Campbell SD, Wevrick R. The Smc5/Smc6/MAGE complex confers resistance to caffeine and genotoxic stress in *Drosophila melanogaster*. PLoS One. 2013;8(3):e59866. doi:10.1371/journal.pone.0059866.

Li G, Zou W, Jian L, Qian J, Deng Y, Zhao J. Non-SMC elements 1 and 3 are required for early embryo and seedling development in Arabidopsis. J Exp Bot. 2017;68(5):1039–1054. doi:10.1093/jxb/erx016.

Li G, Zou W, Jian L, Qian J, Zhao J. AtNSE1 and AtNSE3 are required for embryo pattern formation and maintenance of cell viability during Arabidopsis embryogenesis. J Exp Bot. 2019;70(21):6229–6244. doi:10.1093/jxb/erz373.

Liao G, Jin C, Wang B. Structure and function of the structure maintenance of chromosome (Smc5/6) complex. Guangxi Sci. 2021;28(6):539–546. doi:10.3390/pathogens9100786.

Liu S, Kong D. End resection: a key step in homologous recombination and DNA double-strand break repair. Genome Instab Dis. 2021;2(1):39–50. doi:10.1007/s42764-020-00028-5.

Livak KJ, Schmittgen TD. Analysis of relative gene expression data using real-time quantitative PCR and the $2^{-\Delta\Delta CT}$ method. Methods. 2001;25(4):402–408. doi:10.1006/meth.2001.1262.

López-Sánchez N, González-Fernández Z, Niinobe M, Yoshikawa K, Frade JM. Single mage gene in the chicken genome encodes CMage, a protein with functional similarities to mammalian type II Mage proteins. Physiol Genomics. 2007;30(2):156–171. doi:10.1152/physiolgenomics.00249.2006.

Meier B, Cooke SL, Weiss J, Bailly AP, Alexandrov LB, Marshall J, Raine K, Maddison M, Anderson E, Stratton MR, *et al. C. elegans* whole-genome sequencing reveals mutational signatures related to

carcinogens and DNA repair deficiency. Genome Res. 2014;24(10):1624–1636. doi:10.1101/gr.175547.114.

Mokas S, Mills JR, Garreau C, Fournier MJ, Robert F, Arya P, Kaufman RJ, Pelletier J, Mazroui R. Uncoupling stress granule assembly and translation initiation inhibition. Mol Biol Cell. 2009;20(11):2673–2683. doi:10.1091/mbc.E08.

Odiba AS, Ezechukwu CS, Liao G, Li S, Chen Z, Liu X, Fang W, Jin C, Wang B. Loss of NSE-4 perturbs genome stability and DNA repair in *Caenorhabditis elegans*. Int J Mol Sci. 2022;23(13):7202. doi:10.3390/ijms23137202.

O'Neil NJ, Martin JS, Youds JL, Ward JD, Petalcorin MIR, Rose AM, Boulton SJ. Joint molecule resolution requires the redundant activities of MUS-81 and XPF-1 during *Caenorhabditis elegans* meiosis. PLoS Genet. 2013;9(7):e1003582. doi:10.1371/journal.pgen.1003582.

Palecek J, Vidot S, Feng M, Doherty AJ, Lehmann AR. The Smc5–Smc6 DNA repair complex: bridging of the Smc5–Smc6 heads by the kleisin, nse4, and non-kleisin subunits. J Biol Chem. 2006;281(48):36952–36959. doi:10.1074/jbc.M608004200.

Pebernard S, McDonald WH, Pavlova Y, Yates JR, Boddy MN. Nse1, Nse2, and a novel subunit of the Smc5–Smc6 complex, Nse3, play a crucial role in meiosis. Mol Biol Cell. 2004;15(11):4866–4876. doi:10.1091/MBC.E04-05-0436.

Pebernard S, Wohlschlegel J, McDonald WH, Yates JR, Boddy MN. The Nse5–Nse6 dimer mediates DNA repair roles of the Smc5–Smc6 complex. Mol Cell Biol. 2006;26(5):1617–1630. doi:10.1128/mcb.26.5.1617-1630.2006.

Pradhan B, Kanno T, Umeda Igarashi M, Loke MS, Baaske MD, Wong JSK, Jeppsson K, Björkegren C, Kim E. The Smc5/6 complex is a DNA loop-extruding motor. Nature. 2023;616(7958):843–848. doi:10.1038/S41586-023-05963-3.

Rosu S, Libuda DE, Villeneuve AM. Robust crossover assurance and regulated interhomolog access maintain meiotic crossover number. Science. 2011;334(6060):1286–1289. doi:10.1126/science.1212424.

Sabatella M, Thijssen KL, Davó-Martínez C, Vermeulen W, Lans H. Tissue-specific DNA repair activity of ERCC-1/XPF-1. Cell Rep. 2021;34(2):108608. doi:10.1016/j.celrep.2020.108608.

Saito TT, Youds JL, Boulton SJ, Colaiácovo MP. *Caenorhabditis elegans* HIM-18/SLX-4 interacts with SLX-1 and XPF-1 and maintains genomic integrity in the germline by recombination intermediates. PLoS Genet. 2009;5(11):e1000735. doi:10.1371/journal.pgen.1000735.

Schumacher B, Schertel C, Wittenburg N, Tuck S, Mitani S, Gartner A, Conradt B, Shaham S. *C. elegans* ced-13 can promote apoptosis and is induced in response to DNA damage. Cell Death Differ. 2005;12(2):153–161. doi:10.1038/sj.cdd.4401539.

Schvarzstein M, Pattabiraman D, Libuda DE, Ramadugu A, Tam A, Martinez-Perez E, Roelens B, Zawadzki KA, Yokoo R, Rosu S, *et al.* DNA helicase HIM-6/BLM both promotes mutSγ-dependent crossovers and antagonizes mutSγ-independent interhomolog associations during *Caenorhabditis elegans* meiosis. Genetics. 2014;198(1):193–207. doi:10.1534/genetics.114.161513.

Serrano D, Cordero G, Kawamura R, Sverzhinsky A, Sarker M, Roy S, Malo C, Pascal JM, Marko JF, D'Amours D. The Smc5/6 core complex is a structure-specific DNA binding and compacting machine. Mol Cell. 2020;80(6):1025–1038.e5. doi:10.1016/j.molcel.2020.11.011.

Skibbens RV. Condensins and cohesins—one of these things is not like the other! J Cell Sci. 2019;132(3):jcs220491. doi:10.1242/JCS.220491.

Stamper EL, Rodenbusch SE, Rosu S, Ahringer J, Villeneuve AM, Dernburg AF. Identification of DSB-1, a protein required for initiation of meiotic recombination in *Caenorhabditis elegans*, illuminates a crossover assurance checkpoint. PLoS Genet. 2013;9(8):e1003679. doi:10.1371/journal.pgen.1003679.

Stephan AK, Kliszczak M, Dodson H, Cooley C, Morrison CG. Roles of vertebrate Smc5 in sister chromatid cohesion and homologous recombinational repair. Mol Cell Biol. 2011;31(7):1369–1381. doi:10.1128/MCB.00786-10.

Stephan AK, Kliszczak M, Morrison CG. The Nse2/Mms21 SUMO ligase of the Smc5/6 complex in the maintenance of genome stability. FEBS Lett. 2011;585(18):2907–2913. doi:10.1016/j.febslet.2011.04.067.

Tacer KF, Montoya MC, Oatley MJ, Lord T, Oatley JM, Klein J, Ravichandran R, Tillman H, Kim M, Connelly JP, *et al.* MAGE cancer-testis antigens protect the mammalian germline under environmental stress. Sci Adv. 2019;5(5):eaav4832. doi:10.1126/sciadv.aav4832.

Taylor EM, Copsey AC, Hudson JJR, Vidot S, Lehmann AR. Identification of the proteins, including MAGEG1, that make up the human SMC5-6 protein complex. Mol Cell Biol. 2008;28(4):1197–1206. doi:10.1128/mcb.00767-07.

Toraason E, Salagean AD, Almanzar D, Rog O, Libuda DE. BRCA1/BRC-1 and SMC-5/6 regulate DNA repair pathway engagement in *C. elegans* meiosis. bioRxiv; Prep. Published online June 14, 2022:2022.06.12.495837. doi:10.1101/2022.06.12.495837.

Uhlmann F. SMC complexes: from DNA to chromosomes. Nat Rev Mol Cell Biol. 2016;17(7):399–412. doi:10.1038/nrm.2016.30.

Vermezovic J, Stergiou L, Hengartner MO, Di Fagagna FD. Differential regulation of DNA damage response activation between somatic and germline cells in *Caenorhabditis elegans*. Cell Death Differ. 2012;19(11):1847–1855. doi:10.1038/cdd.2012.69.

Vondrova L, Kolesar P, Adamus M, Nociar M, Oliver AW, Palecek JJ. A role of the Nse4 kleisin and Nse1/Nse3 KITE subunits in the ATPase cycle of SMC5/6. Sci Rep. 2020;10(1):1–13. doi:10.1038/s41598-020-66647-w.

Vujin A, Jones SJ, Zetka M. NHJ-1 is required for canonical nonhomologous end joining in *Caenorhabditis elegans*. Genetics. 2020;215(3):635–651. doi:10.1534/genetics.120.303328.

Ward JD. Rapid and precise engineering of the *Caenorhabditis elegans* genome with lethal mutation co-conversion and inactivation of NHEJ repair. Genetics. 2014;199(2):363–377. doi:10.1534/genetics.114.172361.

Watanabe K, Pacher M, Dukowic S, Schubert V, Puchta H, Schubert I. The structural maintenance of chromosomes 5/6 complex promotes sister chromatid alignment and homologous recombination after DNA damage in *Arabidopsis thaliana*. Plant Cell. 2009;21(9):2688–2699. doi:10.1105/tpc.108.060525.

Weon JL, Potts PR. The MAGE protein family and cancer. Curr Opin Cell Biol. 2015;37:1–8. doi:10.1016/j.ceb.2015.08.002.

Wolters S, Ermolaeva MA, Bickel JS, Fingerhut JM, Khanikar J, Chan RC, Schumacher B. Loss of *Caenorhabditis elegans* BRCA1 promotes genome stability during replication in smc-5 mutants. Genetics. 2014;196(4):985–999. doi:10.1534/genetics.113.158295.

Wozniak KJ, Simmons LA. Hydroxyurea induces a stress response that alters DNA replication and nucleotide metabolism in *Bacillus subtilis*. J Bacteriol. 2021;203(15):171–192. doi:10.1128/JB.00171-21.

Yamaguchi-Iwai Y, Sonoda E, Sasaki MS, Morrison C, Haraguchi T, Hiraoka Y, Yamashita YM, Yagi T, Takata M, Price C, *et al.* Mre11 is essential for the maintenance of chromosomal DNA in vertebrate cells. EMBO J. 1999;18(23):6619–6629. doi:10.1093/emboj/18.23.6619.

Yokoo R, Zawadzki KA, Nabeshima K, Drake M, Arur S, Villeneuve AM. COSA-1 reveals robust homeostasis and separable licensing

and reinforcement steps governing meiotic crossovers. Cell. 2012; 149(1):75–87. doi:10.1016/J.cell.2012.01.052.

Zabrady K, Adamus M, Vondrova L, Liao C, Skoupilova H, Novakova M, Jurcisinova L, Alt A, Oliver AW, Lehmann AR, *et al.* Chromatin association of the SMC5/6 complex is dependent on binding of its NSE3 subunit to DNA. Nucleic Acids Res. 2016;44(3):1064–1079. doi:10.1093/nar/gkv1021.

Zelkowski M, Zelkowska K, Conrad U, Hesse S, Lermontova I, Marzec M, Meister A, Houben A, Schubert V. Arabidopsis NSE4 proteins act in somatic nuclei and meiosis to ensure plant viability and fertility. Front Plant Sci. 2019;10:774. doi:10.3389/fpls.2019.00774.

Zhou Z, Hartwieg E, Robert Horvitz H. CED-1 is a transmembrane receptor that mediates cell corpse engulfment in *C. elegans*. Cell. 2001;104(1):43–56. doi:10.1016/S0092-8674(01)00190-8.

Editor: J. Engebrecht